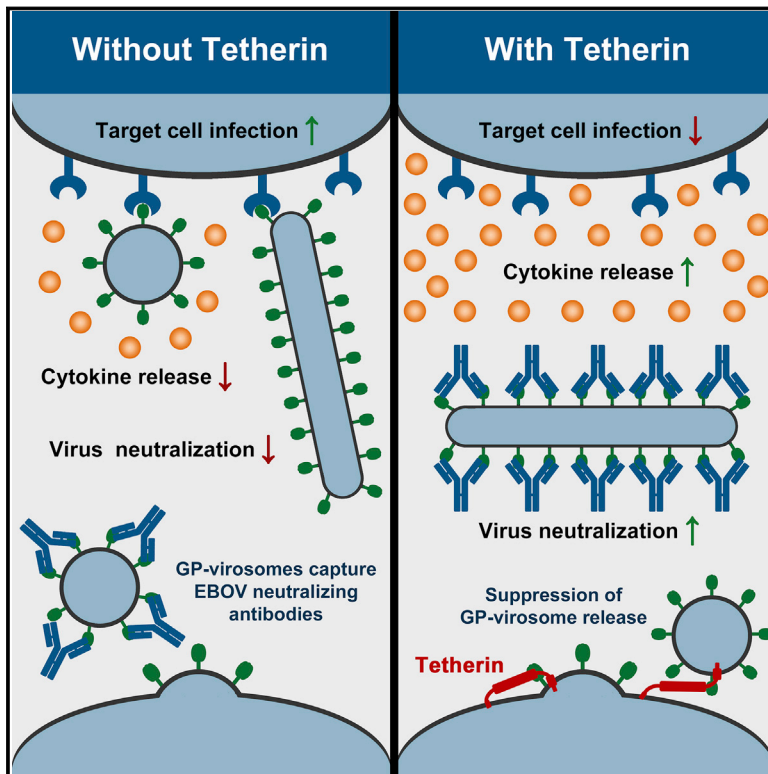


Cell Reports

Release of Immunomodulatory Ebola Virus Glycoprotein-Containing Microvesicles Is Suppressed by Tetherin in a Species-Specific Manner

Graphical Abstract



Authors

Julia Nehls, Ramona Businger, Markus Hoffmann, ..., Stephan Hailfinger, Stefan Pöhlmann, Michael Schindler

Correspondence

michael.schindler@med.uni-tuebingen.de

In Brief

Nehls et al. demonstrate that the glycoprotein of the highly pathogenic Ebola virus is incorporated into secretory vesicles, called GP-virosomes, to dampen the immune response and capture neutralizing antibodies. The lack of replication competence and the incorporation of antigenically intact GP might qualify GP-virosomes as safe vaccine candidates.

Highlights

- The Ebola virus glycoprotein (GP) drives the release of GP-containing virosomes
- Tetherin restricts GP-virosome release through transmembrane domain interactions
- GP-virosome release is most efficient for GPs of highly pathogenic Ebola viruses
- Immunomodulatory GP-virosomes serve as decoys for EBOV-neutralizing antibodies



Nehls et al., 2019, Cell Reports 26, 1841–1853
February 12, 2019 © 2019 The Author(s).
<https://doi.org/10.1016/j.celrep.2019.01.065>

CellPress

Release of Immunomodulatory Ebola Virus Glycoprotein-Containing Microvesicles Is Suppressed by Tetherin in a Species-Specific Manner

Julia Nehls,^{1,2} Ramona Businger,¹ Markus Hoffmann,³ Constantin Brinkmann,³ Birgit Fehrenbacher,⁴ Martin Schaller,⁴ Brigitte Maurer,¹ Caroline Schönfeld,⁵ Daniela Kramer,⁵ Stephan Hailfinger,⁵ Stefan Pöhlmann,³ and Michael Schindler^{1,2,6,*}

¹Institute of Medical Virology and Epidemiology of Viral Diseases, University Hospital Tübingen, 72076 Tübingen, Germany

²Institute of Virology, Helmholtz Zentrum München, German Research Center for Environmental Health, 85764 Neuherberg, Germany

³Infection Biology Unit, German Primate Center, 37077 Göttingen, Germany

⁴Department of Dermatology, University Hospital Tübingen, 72076 Tübingen, Germany

⁵Interfaculty Institute for Biochemistry, University of Tübingen, 72076 Tübingen, Germany

⁶Lead Contact

*Correspondence: michael.schindler@med.uni-tuebingen.de

<https://doi.org/10.1016/j.celrep.2019.01.065>

SUMMARY

The Ebola virus glycoprotein (EBOV-GP) forms GP-containing microvesicles, so-called virosomes, which are secreted from GP-expressing cells. However, determinants of GP-virosome release and their functionality are poorly understood. We characterized GP-mediated virosome formation and delineated the role of the antiviral factor tetherin (BST2, CD317) in this process. Residues in the EBOV-GP receptor-binding domain (RBD) promote GP-virosome secretion, while tetherin suppresses GP-virosomes by interactions involving the GP-transmembrane domain. Tetherin from multiple species interfered with GP-virosome release, and tetherin from the natural fruit bat reservoir showed the highest inhibitory activity. Moreover, analyses of GP from various ebolavirus strains, including the EBOV responsible for the West African epidemic, revealed the most efficient GP-virosome formation by highly pathogenic ebolaviruses. Finally, EBOV-GP-virosomes were immunomodulatory and acted as decoys for EBOV-neutralizing antibodies. Our results indicate that GP-virosome formation might be a determinant of EBOV immune evasion and pathogenicity, which is suppressed by tetherin.

INTRODUCTION

The Ebola virus (EBOV) is a highly pathogenic virus and the causative agent of a severe and systemic infection, the EBOV disease (EVD) (Baseler et al., 2017). EBOV is a zoonotic virus, and fruit bats are proposed to constitute a natural reservoir (Buceta and Johnson, 2017; Pourrut et al., 2009). Since its discovery, sporadic and self-limiting outbreaks occurred primarily in remote villages of central Africa. However, the 2014–2016 EVD epidemic in West Africa demonstrated that introduction of the virus into

densely populated regions can have devastating consequences (Kalra et al., 2014) and that EVD constitutes a major health threat.

EBOV is the prototype member of the genus *Ebolavirus* within the family *Filoviridae*, which contains a total of five different species of ebolaviruses. The members of these species differ substantially in pathogenicity: the species *Zaire ebolavirus* contains a single member, EBOV, which is associated with case-fatality rates of up to 88% and is responsible for the majority of past EVD outbreaks. The species *Sudan ebolavirus* (of which the only member is Sudan virus [SUDV]) and *Bundibugyo ebolavirus* (of which the only member is Bundibugyo virus [BDBV]) contain strains that can also cause fatal disease in humans (Towner et al., 2008). Infection with Taï Forest virus (TAFV; the only member of the species *Taï Forest ebolavirus*) was associated with a single case of EVD, but the afflicted patient survived (Le Guenno et al., 1995). Reston virus (RESTV), the only member of the species *Reston ebolavirus*, has first been detected in non-human primates displaying signs of EVD but apparently does not cause disease in humans (de La Vega et al., 2015).

EBOV is enveloped by a lipid membrane and harbors a negative-sense single-stranded RNA genome comprising seven viral genes that code for at least nine viral proteins. The only protein that is exposed on the viral surface is the glycoprotein (GP), which is crucial for host cell attachment and membrane fusion. Following cotranslational import into the endoplasmic reticulum, the GP is trafficked through the constitutive secretory pathway, where it is extensively N- and O-glycosylated and cleaved into two subunits, GP1 and GP2, by the host cell protease furin (Lee and Saphire, 2009; Mühlberger, 2007). Trimers of GP are inserted into the plasma membrane at viral budding sites, where it is incorporated into assembling particles, such that the GP trimers protrude as spikes from the viral lipid membrane.

In mature GP, the GP1 and GP2 subunits are covalently associated via two disulfide bonds. The GP1 subunit has a molecular weight of approximately 130 kDa and is composed of the receptor-binding domain (RBD), a glycan cap (which is extensively modified with N-glycans) and a highly O-glycosylated mucin-like domain (MLD). The GP2 subunit is ~22 kDa in size and includes the fusion peptide, a transmembrane domain (TMD), and a short cytoplasmic tail (Lee and Saphire, 2009). However,



surface GP is not the primary gene product of GP. The mRNA encoding surface GP is generated because of stuttering of the viral RNA-dependent RNA polymerase, which leads to a frameshift. It has been suggested that this RNA-editing mechanism is important to limit cytotoxic effects imposed by surface GP (Volchkov et al., 2001). The primary product of the GP gene is a 55 kDa form of GP, soluble GP (sGP), which shares only the N-terminal part with surface GP1 (Lee and Saphire, 2009; Sanchez et al., 1996). Following translation, soluble GP forms dimers that are secreted from the host cell (Volchkova et al., 1998). It has been proposed that soluble GP serves as a decoy for neutralizing anti-GP antibodies (Ito et al., 2001). However, this hypothesis is controversial, because the tertiary structure of soluble GP most likely differs substantially from the structure of surface GP (Lee and Saphire, 2009; Ning et al., 2017).

Besides host cell attachment and entry, surface GP has been found to interact and interfere with the host restriction factor tetherin (Kaletsky et al., 2009; Kupzig et al., 2003). Tetherin (BST2, CD317) is an antiviral interferon-regulated gene and part of the innate immune system (Neil et al., 2008; Sauter, 2014; Van Damme et al., 2008). It is a type II transmembrane protein that forms dimers and adopts a highly unusual topology at the plasma membrane. It is composed of two membrane anchors, a C-terminal GPI anchor and an N-terminal TMD, which are linked by a coiled-coil ectodomain. This unique structure allows tetherin to trap budding virions at the cell surface by inserting one membrane anchor into the viral envelope while the second membrane anchor remains inserted into the plasma membrane of the cell. Consequently, tetherin physically links newly synthesized virus particles to the host cell and thereby prevents their transmission to neighboring cells (Sauter, 2014). Tetherin restricts a large variety of enveloped viruses (Mahauad-Fernandez and Okeoma, 2015), and a recent study suggests that tetherin also acts on exosome release (Edgar et al., 2016).

The third GP product is the small secretory GP (ssGP). ssGP is produced at only very low levels (Volchkova et al., 1998) because of transcriptional editing, and its biological activities are unknown (Mehedi et al., 2011). An additional form of GP, shedGP, is released from the host upon ADAM17/TACE-mediated proteolytic cleavage of surface GP at the plasma membrane (Dolnik et al., 2004). ShedGP has been suggested to contribute to viral pathogenicity as it might trap neutralizing GP antibodies and promote vascular permeability (Escudero-Pérez et al., 2014). Furthermore, GP shedding might regulate surface levels of GP and thus viral cytotoxicity (Dolnik et al., 2015).

The release of exosomes or microvesicles carrying viral proteins or nucleic acids has been reported upon infection with diverse viruses, including HIV-1, hepatitis C virus (HCV), herpes simplex virus (HSV), Epstein-Barr virus (EBV), and hepatitis B virus (HBV) (Chahar et al., 2015; Hu and Liu, 2017; Meckes and Raab-Traub, 2011). It has been suggested that viruses take advantage of these vesicles because of their contribution to viral persistence, viral dissemination, and immune evasion (Chahar et al., 2015; Lai et al., 2015; Meckes and Raab-Traub, 2011). Microvesicles, which bear GP and are termed virosomes, are also released in the context of EBOV infection (Volchkov et al., 1998), but their role in viral pathogenesis is unknown.

In this study, we investigated whether GP-containing microvesicles could be a determinant of EBOV pathogenicity and analyzed determinants of GP-virosome release. We furthermore hypothesized that tetherin, besides inhibiting release of progeny viral particles, might also interfere with the release of GP-virosomes. We found that GPs from highly pathogenic EBOV strains were more potently released in virosomes compared with GPs from less pathogenic strains. Moreover, GP-virosomes trapped anti-GP antibodies and protected viral particles from neutralization. Finally, GP-virosome release was potently suppressed by tetherin through specific interaction with the GP-TMD. Hence, tetherin has the capacity to block secretion of virus protein-containing microvesicles and might thereby help suppress viral pathogenicity independent from its inhibitory effects on particle release.

RESULTS

EBOV-GP Is Released in a Microvesicle-Associated Manner as Virosomes

We first aimed to verify that GP is released from GP-expressing cells in a microvesicle-associated manner. For this, we used a centrifugation protocol that should pellet vesicle-associated GP from cell culture supernatants, but not shedGP (Dolnik et al., 2004; Volchkov et al., 1998). To confirm the selective enrichment of GP-containing vesicles, we transfected 293T cells to express GP, pelleted the supernatants, and performed immunoblotting with GP1- and GP2-specific antibodies. In cells and supernatants, GP1 runs at ~130 kDa, as expected (Figure 1A). Furthermore, cell-associated GP2 as well as GP2 in the supernatant exhibited the same size of ~22 kDa (Figure 1A). This corresponds to GP2 from the full-length form of surface GP instead of shedGP, which would have a smaller GP2 subunit (14 kDa) because of TACE cleavage (Dolnik et al., 2004).

We then intended to directly prove the presence of GP-bearing vesicles in the supernatant of GP-transfected cells according to a previously published experimental approach by Volchkov et al. (1998). To this end, we prepared a linear sucrose gradient and overlaid the gradient with the supernatant of GP-expressing 293T cells with or without the addition of Triton X-100 (Figure 1B). Following ultracentrifugation, we unloaded ten fractions from the bottom to the top with decreasing sucrose concentration and subjected the fractions to western blot analysis. In the absence of Triton X-100, full-length GP (detected as GP1) is found in fractions 5–10, with the highest levels of GP being present in fraction 10 (Figure 1B). Of note, we also detected soluble GP, which is the primary gene product when GP is produced in the viral context. Here, when we express full-length GP from a transfected plasmid, the cellular DNA-dependent RNA polymerase might also produce a minor fraction of soluble GP mRNAs because of stuttering, similar to previous observations (Gnirß et al., 2014; Mohan et al., 2012; Vande Burgt et al., 2015; Volchkov et al., 2001). Soluble GP was predominantly present in fractions 5–7. In the presence of Triton X-100, GP was also detectable in fractions 5–10, but the highest levels of GP were present in fractions 7, 8, and 9 (Figure 1B). This finding confirms that GP is vesicle associated, as because of their size and complexity,

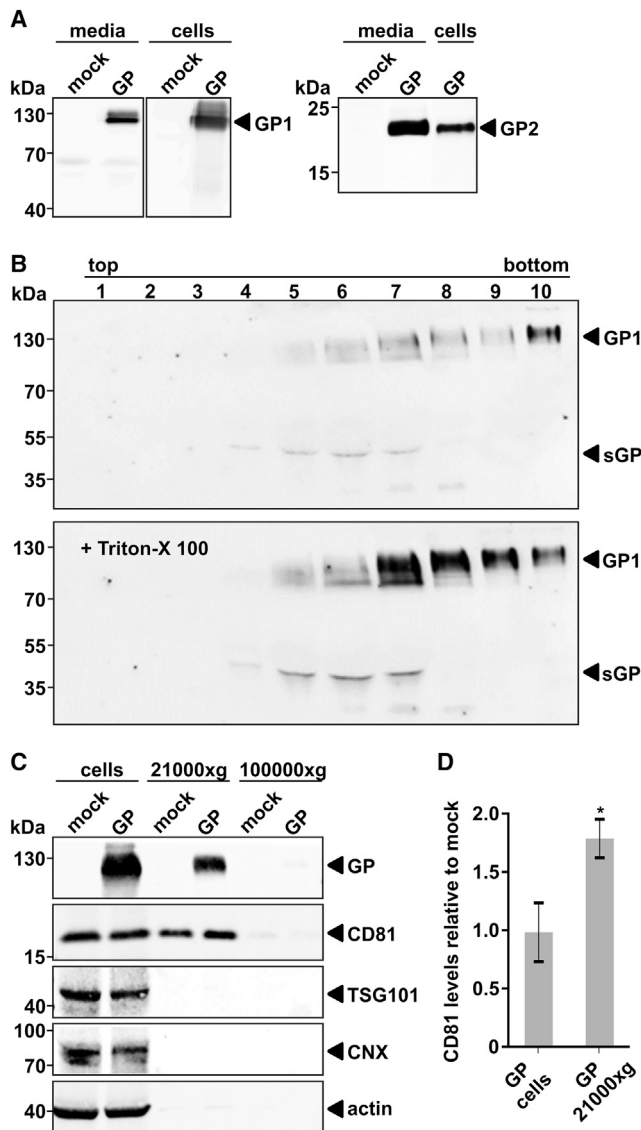


Figure 1. EBOV-GP Is Released from GP-Expressing Cells in a Vesicle-Associated Manner

(A) 293T cells were transfected to express Ebola virus-glycoprotein (EBOV-GP). 24 hours post-transfection (hpt), supernatants were harvested and purified with a protocol that pellets vesicles and virus-like particles (see STAR Methods). GP1 and GP2 in the purified media and cell lysates were analyzed using western blot.

(B) 293T cells were transfected with EBOV-GP. 24 hours post-transfection, a linear sucrose gradient was established and overlaid with the cell culture supernatant of the GP-transfected cells. The supernatant was either left untreated (top) or treated with 1% Triton X-100 (bottom). The supernatants were subsequently centrifuged at $50,000 \times g$ for 2 h at 4°C . Afterward, ten fractions were collected from the bottom (fraction 10) to the top (fraction 1) of the gradient. The GP levels within the ten fractions were then analyzed using western blot using a rabbit serum that targets the GP1 subunit.

(C) Supernatants of 293T cells were treated as in (A), but two sequential centrifugation steps were done to collect vesicles that pellet at $21,000 \times g$ or $100,000 \times g$. Purified media and cells analyzed using western blot for exosomal (CD81, TSG101) and cellular (CNX, actin) markers as well as GP.

(D) Densitometric quantification of CD81 levels from four independent experiments. For each experiment, values for CD81 levels in cells and supernatants

secretory vesicles move toward the bottom of a sucrose gradient. In the presence of detergent, the vesicles are disrupted, which leads to a broader distribution of GP throughout the sucrose gradient. In case of non-vesicle-associated shedGP (which is released by proteolytic cleavage), we would expect no difference in the abundance of GP after the addition of Triton X-100, as is the case for soluble GP (Figure 1B). GP-containing microvesicles could represent a fraction of exosomes that incorporate GP. To analyze this, we first fractionated cell culture supernatants by ultracentrifugation, which should allow to discriminate exosomes and smaller vesicles (<100 nm, pelleted at $100,000 \times g$) from microvesicles ($100\text{--}1,000$ nm, pelleted at $21,000 \times g$; Szatanek et al., 2015; Thery et al., 2006; Witwer et al., 2013). Then, we blotted for marker proteins that should be specifically enriched (CD81, TSG101), underrepresented, or absent (calnexin [CNX], actin) (Lötvald et al., 2014) as well as for GP (Figure 1C). Enrichment of GP in the $21,000 \times g$ fraction and co-detection of CD81, but not TSG101, CNX, or actin indicates that GP-virosomes are non-exosomal extracellular vesicles with a size larger than 100 nm. Furthermore, we observed moderately elevated levels of CD81 in supernatants of GP-expressing cells compared with mock-transfected cells (Figure 1D). In conclusion, our approach allows specific analysis of GP-virosomes, which are non-exosomal CD81-positive extracellular microvesicles.

Visual Characterization of GP-Virosomes and Their Release

We next thought to visualize GP-virosomes in EBOV relevant target cells (i.e., myeloid cells) (Dahlmann et al., 2015; Ströher et al., 2001; Wahl-Jensen et al., 2011) and HeLa cells, which are a model cell line for the release of extracellular vesicles (Edgar et al., 2016) and EBOV infection (Bhattacharyya et al., 2010; Dahlmann et al., 2015; Dolnik et al., 2004). For this, we generated lentiviral vectors expressing EBOV-GP or EBOV-GP fused with GFP. PMA-differentiated macrophage-like THP-1 cells and HeLa cells transduced with the GP-expressing lentivirus released GP-virosomes, as expected (Figure 2A and data not shown). Analysis of GP-GFP expressing cells by three-dimensional (3D) structured illumination microscopy (SIM) live-cell imaging revealed multiple GP-containing vesicles associated with the vicinity of the plasma membrane (PM) (Figure 2B). GP-virosomes were highly dynamic, released from the plasma membrane within $20\text{--}40$ s (Figure 2C; Videos S1, S2, S3, and S4) and showed large heterogeneity with sizes of ~ 200 nm in macrophage-like THP-1 and $\sim 300\text{--}500$ nm in HeLa cells (Figures 2D, 2E, S1, and S2). These observations are in line with the sedimentation of GP-virosomes at $21,000 \times g$ (Figure 1C) and were further corroborated by inspection of GP-expressing cells with electron microscopy (Figures 2F–2H). In comparison with vesicular structures released from control cells (Figures 2I–2L and S3), GP-virosomes were highly enriched and had a high density of

from GP-expressing cells were divided by the corresponding CD81 level in mock cells and supernatants. Statistical significance was tested using a two-tailed, unpaired Mann-Whitney test ($p < 0.05$); data are mean \pm SD.

One representative of three (A and B) and four (C) independent experiments is shown, respectively.

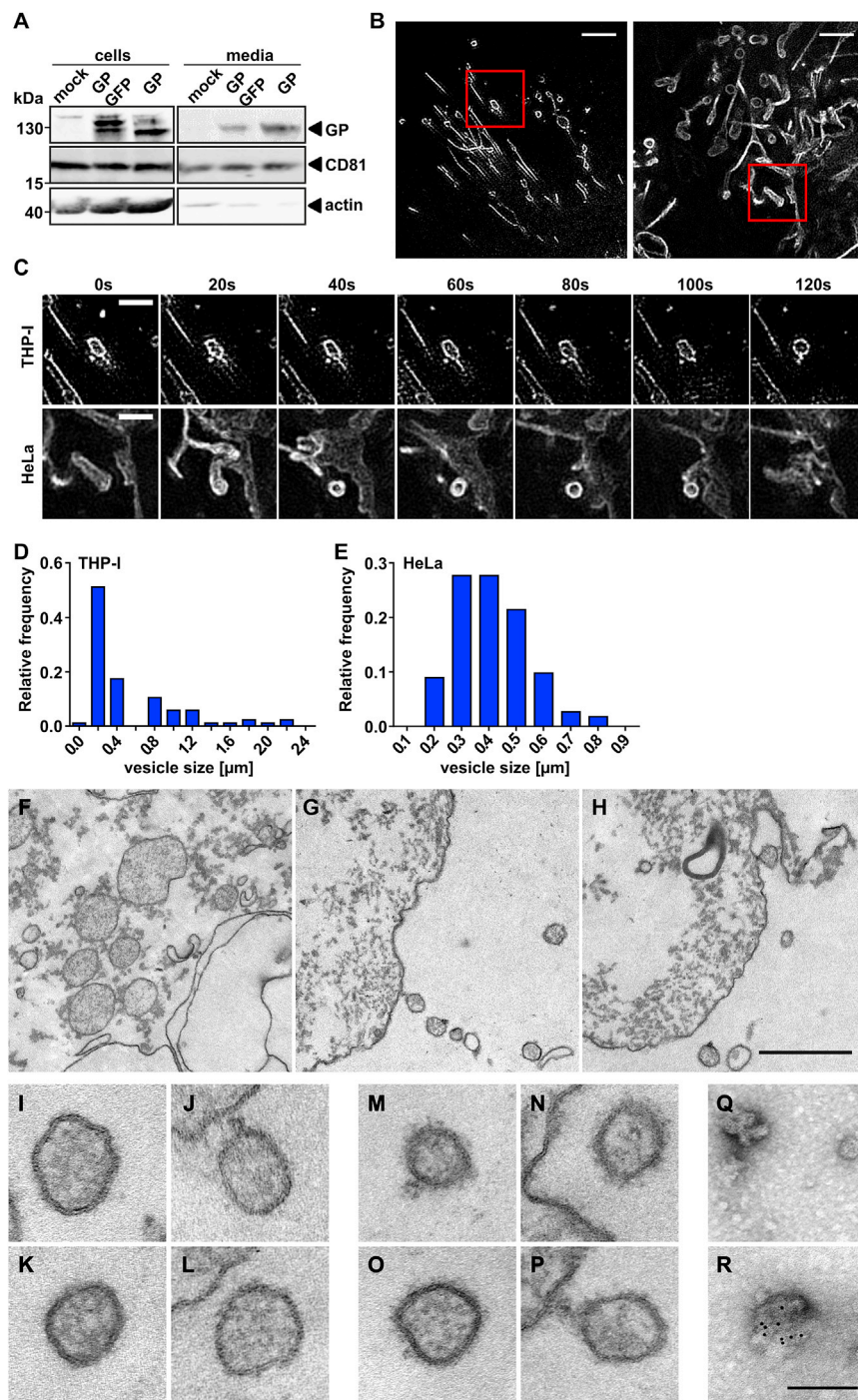


Figure 2. Visual Characterization of GP-Virosomes

(A) PMA-differentiated THP-1 cells were transduced with parental lentiviral vectors (mock) or lentiviral vectors expressing either GP fused to GFP or GP only. Cells and supernatants were harvested 72 h later and analyzed using western blot for the presence of GP, CD81, and actin. Shown is one representative of three experiments. (B) Three-dimensional (3D) SIM live-cell imaging of GP-GFP transduced THP-1 (left) or HeLa cells (right) at 3 days post-infection (dpi). Shown is the start of the imaging series at a membrane-proximal region. Recorded stacks are presented at maximum intensity projections (MIPs). Scale bar, 2 μ m.

(C) Time lapse of the magnified areas indicated in (B). 3D SIM live-cell imaging in 20 s intervals. Recorded stacks are presented at MIP. Top: THP-1; bottom: HeLa cells. Scale bar, 1 μ m. See also Videos S1, S2, S3, and S4.

(D and E) Heterogeneity and relative vesicle size distribution of GP-virosomes in (D) THP-1 (n = 86) and (E) HeLa cells (n = 112). For examples of size measurements, see Figure S1 (THP-1) and Figure S2 (HeLa).

(F–R) Transmission electron microscopy of GP-expressing HeLa cells (F–H) and (I–L) vesicles from mock cells or (M–P) GP-expressing cells as well as negative staining and immuno-gold electron microscopy (EM) against GP for vesicles isolated from (Q) mock or (R) GP-expressing cells. Scale bars, 500 nm (F–H) and 100 nm (I–R).

See also Figure S3 for representative images of non-GP-expressing control HeLa cells and Figure S4 for immuno-gold EM of vesicles isolated from mock or GP-expressing cells.

membrane-associated GP (Figures 2M–2P), as also evident from immuno-gold staining of vesicles from mock cells (Figure 2Q) versus GP-virosomes (Figure 2R; see also Figure S4).

Tetherin Restricts the Release of EBOV-GP-Virosomes

Release of GP-virosomes is reminiscent of viral particles budding from the plasma membrane (Figure 2). We hence analyzed whether tetherin affects the release of GP-bearing viro-

somes. For this, we transfected 293T cells to express tetherin and GP and monitored formation of GP-virosomes in cell culture supernatants (Figure 3A). Of note, just 50 ng of transfected tetherin plasmid led to a dramatic reduction in released GP-virosomes, and this reduction increased in a concentration-dependent manner (Figure 3A). Next, we tested HeLa cells, which express endogenous tetherin. Also in this cell system, additional expression of tetherin via transfection resulted in reduced GP-virosome release (Figure 3B). Tetherin overexpression could have side effects on cellular

pathways artificially affecting GP processing. We therefore transfected HeLa cells to express GP, performed small interfering RNA (siRNA) knockdown of endogenous tetherin and monitored release of GP-virosomes relative to cells treated with a scrambled control siRNA (si-scr). In line with our overexpression experiments, siRNA knockdown of tetherin led to increased release of GP-virosomes (Figure 3C). Altogether, GP is secreted in microvesicles in the absence of other EBOV

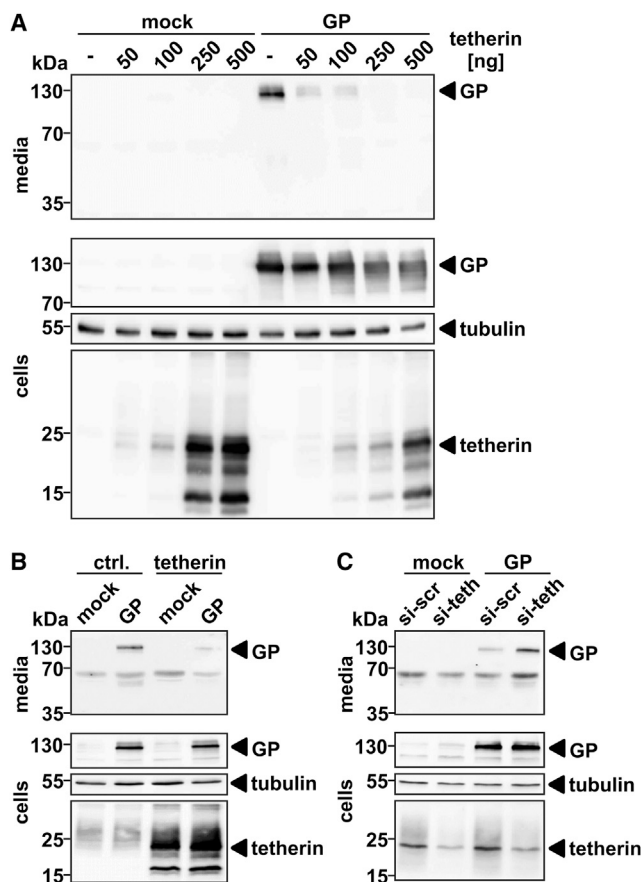


Figure 3. Tetherin Suppresses the Release of EBOV-GP

(A) 293T cells were transfected to express EBOV-GP or an empty control plasmid (mock) and increasing amounts of tetherin. 24 hours post-transfection, GP levels in the media and in the cell lysates as well as tetherin levels in the cell lysates were determined using western blot.

(B) HeLa cells were transfected to express EBOV-GP and tetherin or an empty control plasmid. 24 hours post-transfection, cell culture media as well as cell lysates were analyzed as described in (A).

(C) HeLa cells were transfected with a tetherin-specific or a non-targeting siRNA as control. 24 hours later, the cells were additionally transfected to express GP or a non-coding control plasmid. After another 24 h, GP and tetherin steady-state levels in cell culture media and in cell lysates were analyzed using western blot. The results were verified in at least three additional experiments.

proteins and tetherin has the capacity to suppress the release of these virosomes.

Suppression of GP-Virosome Release Is Mediated by the Tetherin GPI Anchor and Modulated by Its Primary Sequence

The unique tertiary structure of tetherin, which comprises two membrane anchors, is crucial for tetherin's ability to restrict the release of virus particles from the cell surface, while its primary amino acid sequence is not important (Perez-Caballero et al., 2009). We therefore asked whether tetherin-mediated suppression of GP-virosome release also depends on its unique topology. For this, we generated three tetherin mutants lacking the

C-terminal GPI anchor (Δ GPI), the TMD (Δ TMD), or both membrane anchors. When 293T cells were transfected to express GP and the various tetherin mutants, only WT tetherin was able to restrict virosome release. Furthermore, upon deletion of tetherin's GPI anchor, we could measure robust incorporation of tetherin into GP-virosomes (Figure 4A). This strongly suggests that tetherin arrests GP-virosomes at the plasma membrane by inserting its TMD in the virosome membrane and the GPI anchor into the plasma membrane. Deletion of the TMD also abrogated tetherin's ability to suppress release of GP-virosomes. However, loss of the TMD also resulted in loss of the tetherin-specific glycosylation pattern (Figure 4A). Closer examination of tetherin localization by confocal microscopy furthermore revealed mislocalization of the tetherin Δ TMD and the double mutant (Figure 4B), precluding a clear conclusion from this result.

Next, we wondered whether tetherin orthologs from different species that have low sequence homology with human tetherin but adopt the same conformation, are able to suppress GP-virosome release (Heusinger et al., 2015). 293T cells were transfected to express human, hamster, or alligator tetherin as well as GP and analyzed for GP-virosome release (Figure 4C). Hamster and alligator tetherin restricted GP-virosome release, but with differential efficiency. Hamster tetherin was expressed in similar amounts than human tetherin but was slightly less active in inhibiting GP-virosomes, whereas alligator tetherin was expressed in lower levels but had a similar restricting activity in comparison with human tetherin. We extended this analysis to an artificial tetherin construct that is composed of the transferrin receptor TMD, the DMPK ectodomain, and the uPAR GPI anchor (Perez-Caballero et al., 2009) and tetherin from fruit bat species *Epomops buettikoferi* and *Hypsignathus monstrosus*. These have been previously proposed to constitute the EBOV's natural reservoir, in which the virus persists presumably without causing disease (Figure 4D) (Pourrut et al., 2009). Not only human tetherin but also artificial tetherin and both fruit bat tetherin constructs suppressed the release of GP-virosomes (Figure 4D). Again, there was a sequence specific element, because the artificial tetherin variant was expressed to very high levels but was only slightly more active than human tetherin. Of note, both fruit bat tetherin constructs suppressed release of GP-virosomes in a highly efficient manner.

Taken together, these results demonstrate that tetherin suppresses GP-virosome release via its GPI anchor and its unique topology. However, the efficiency of the restrictive activity is also modulated by the primary tetherin sequence and varies between tetherin from different species.

The RBD and TMD of EBOV-GP Are Determinants of GP-Virosome Release

To elucidate which GP residues or domains are required for the release of GP-virosomes, we analyzed a set of previously characterized GP mutants containing single amino acid substitutions in the RBD (F88A, L111A, L122A, and W104A) (Brinkmann et al., 2016; Manicassamy et al., 2005; Martinez et al., 2013) or mutation of a conserved GXXXA motif in the TMD (LXXXL) (González-Hernández et al., 2018; Hacke et al., 2015). 293T cells were transfected to express the various GP variants and GP-virosome release in cell culture supernatants was analyzed using western

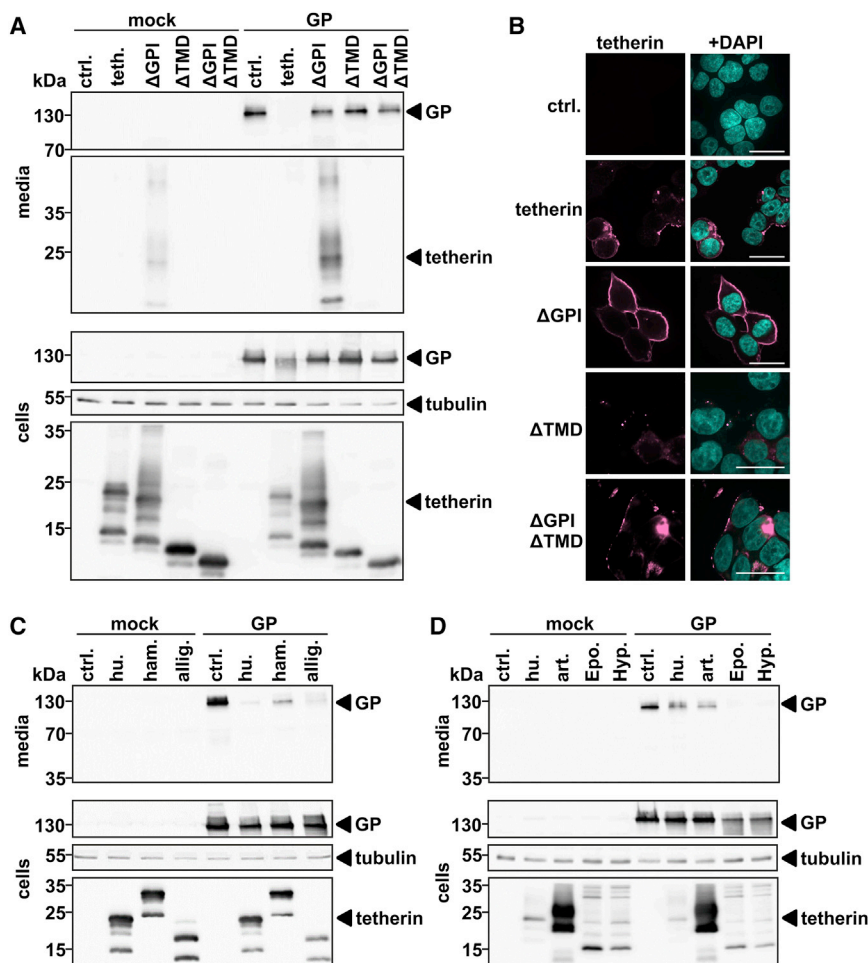


Figure 4. Determinants in Tetherin Important for Suppression of EBOV-GP Release

(A) 293T cells were transfected to express EBOV-GP or a control plasmid and wild-type tetherin or the indicated tetherin mutants. 24 hours post-transfection, GP and tetherin levels in cell culture media and cell lysates were determined using western blot.

(B) Representative confocal fluorescence images of 293T cells that were transfected to express the indicated tetherin variants. Tetherin was detected with a specific antibody and counterstained with an Alexa 633-conjugated secondary antibody. Nuclei of cells were visualized by DAPI. Scale bar, 40 μm.

(C) 293T cells were transfected to express EBOV-GP or a control plasmid as well as Flag-tagged human (hu.), hamster (ham.), or alligator (allig.) tetherin. 24 hours post-transfection, GP levels in cell culture media and cell lysates as well as tetherin levels in the cell lysates were determined using western blot.

(D) Same setup as in (C), but 293T cells were transfected to express HA-tagged human tetherin, artificial (art.) tetherin, *Epomops franqueti* (Epo.) tetherin, or *Hypsignathus monstrosus* (Hyp.) tetherin together with GP or a non-coding control plasmid. All results presented were verified in at least three additional independent experiments.

blot (Figure 5A). GP mutants F88A, L111A, and L122A were strongly impaired in their capacity to induce GP-virosomes, whereas the W104A mutant had wild-type (WT)-like activity, similar to the GXXXA motif changed to LXXXL. Formation of virosomes by the mutants was sensitive toward tetherin overexpression (Figure 5A) and the whole phenotype could be recapitulated in HeLa cells, expressing endogenous tetherin levels (Figure 5B). In line with our previous result (Figure 3C), tetherin knockdown in HeLa cells elevated GP-virosome release of WT EBOV-GP, the W104A and LXXXL mutant. In contrast, tetherin depletion did not lead to enhanced GP-virosome release of the F88A, L111A, and L122A variants (Figure 5B). Hence, impaired GP-virosome formation of the three RBD mutants in comparison with WT GP is functionally unrelated to the expression of tetherin.

We have previously shown that tetherin directly interacts with GP, and this interaction is most likely mediated via the GP-TMD, as demonstrated in cells overexpressing tagged GP and tetherin variants (Kühl et al., 2011). Hence, transmembrane interactions might be involved in suppression of GP-virosomes by tetherin. To test for this, we used a chimeric EBOV-GP variant (ELE) in which the TMD was replaced with that of the heterologous Lassa virus (LASV) GPC (Gnirß et al., 2014). Indeed, in

HeLa cells, interaction between endogenous tetherin and the GP-ELE variant was impaired, but not fully disrupted, suggesting that the GP-TMD participates in tetherin binding (Figure 5C). Furthermore, WT GP localization, in contrast to the chimeric ELE variant, was more defined at the plasma membrane and showed intense tetherin colocalization in this region (Figure 5D). We additionally performed co-immunoprecipitation in 293T cells transfected to express tetherin and V5-tagged GP variants (Figure 5E). EBOV-GP and the ELE variant immunoprecipitated tetherin, whereas the LASV-GPC did not. Of note, upon replacement of the TMD in the LASV-GPC with that of EBOV-GP (LEL), the chimeric GP-LEL was capable to interact with tetherin (Figure 5E), supporting an important role of the EBOV-GP-TMD in tetherin interaction.

When we transfected 293T cells to express WT GP or the chimeric ELE variant, the capability of both variants to secrete GP-virosomes was sensitive to tetherin overexpression (Figure 5F). This finding is not surprising, considering that the ELE variant is impaired, but not completely defective in tetherin binding (Figures 5C and 5E). In contrast, when we moved to HeLa cells expressing endogenous tetherin, GP-virosome formation by WT GP was impaired by tetherin, whereas ELE-chimera virosomes were released in a tetherin-independent manner (Figure 5G).

Altogether, residues in the RBD of the EBOV-GP as well as transmembrane interactions of GP with tetherin are determinants of GP-virosome formation and release.

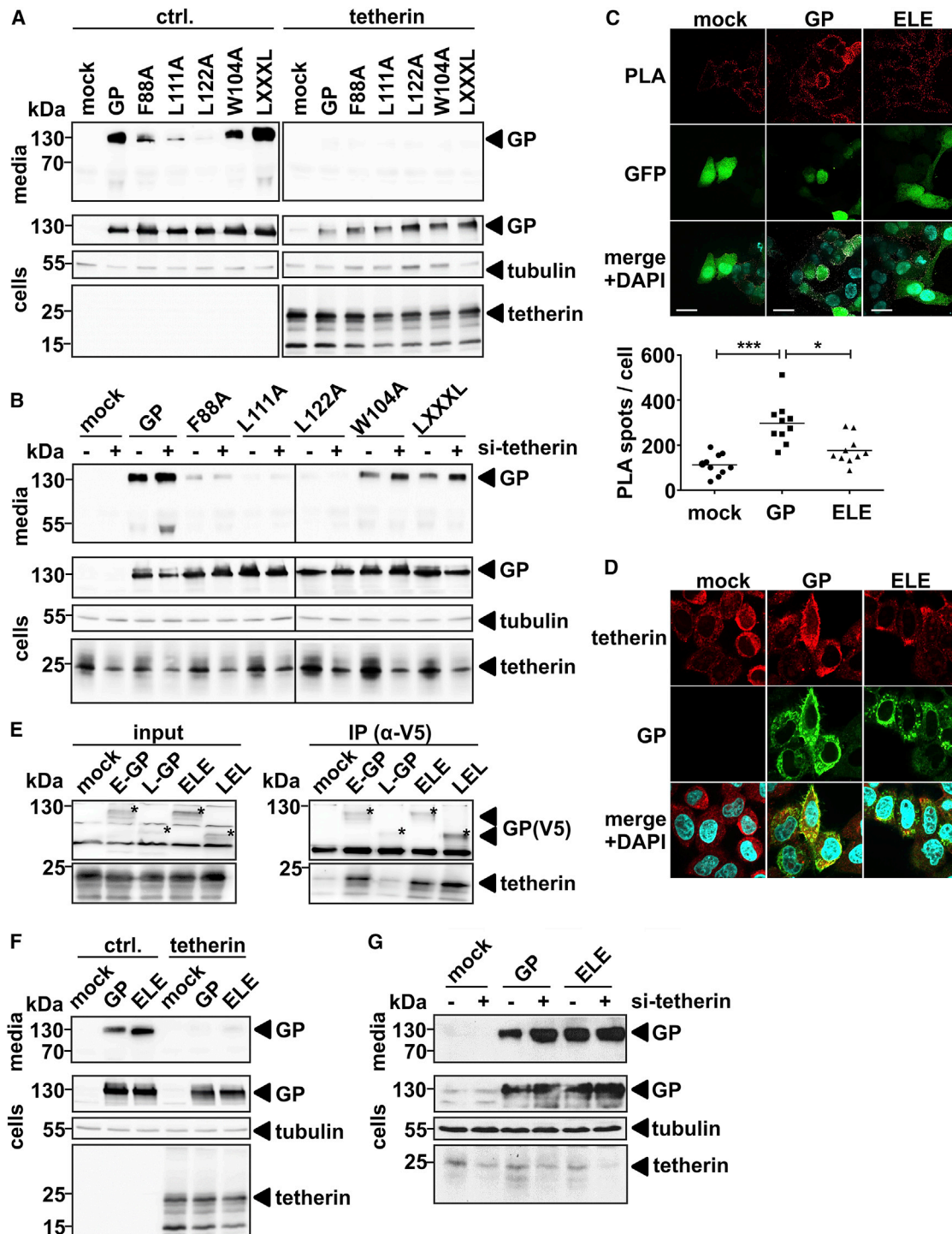


Figure 5. The EBOV-GP RBD and TMD Are Determinants of GP Release

(A) 293T cells were transfected to express EBOV-GP or the indicated GP mutants together with tetherin or a non-coding control plasmid. 24 hours post-transfection, GP levels in cell culture media and cell lysates as well as tetherin levels in cell lysates were analyzed using western blot.

(B) HeLa cells were transfected to express EBOV-GP or the indicated GP mutants together with a tetherin-specific siRNA or a non-targeting siRNA as negative control. 24 hours post-transfection, GP levels in cell culture media and cell lysates as well as tetherin levels in cell lysates were analyzed using western blot.

(C) HeLa cells were transfected to express EBOV-GP or the ELE variant together with GFP from a bicistronic plasmid or the respective control plasmid only expressing GFP (mock). 24 hours post-transfection, a proximity ligation assay was performed with antibodies against EBOV-GP1 and tetherin, respectively.

(legend continued on next page)

GP from Highly Pathogenic EBOV Strains Is Efficiently Secreted in Virosomes

To obtain insight into the potential importance of GP-virosome formation for EBOV pathogenicity, we analyzed the extent of GP-virosome release among four ebolavirus species. EBOV, SUDV, TAFV, and RESTV differ concerning their pathogenicity, with EBOV being the most pathogenic variant and RESTV presumably being non-pathogenic in humans (de La Vega et al., 2015). For this, we transfected 293T cells to express EBOV-, SUDV-, TAFV-, and RESTV-GP, respectively, and co-transfected tetherin or a control plasmid (Figure 6A). EBOV-GP expression resulted in more efficient release of GP-virosomes in comparison with SUDV-GP and TAFV-GP, which released GP-virosomes in an almost undetectable manner. RESTV-GP-virosome formation was lower compared with EBOV-GP but clearly higher than that mediated by SUDV- or TAFV-GP. Upon tetherin co-expression, only EBOV-GP facilitated some weak residual virosome release, indicating that tetherin has the potential to restrict the release of secretory GP vesicles from all the tested ebolavirus species. Furthermore, in the context of endogenous tetherin expression in HeLa cells, only GP from the highly pathogenic EBOV strain efficiently released virosomes into the cell culture supernatants (Figure 6B).

To further challenge the hypothesis that the release of GP-virosomes might be a determinant of EBOV pathogenicity, we analyzed a GP mutant that naturally arose during the 2014–2016 West Africa outbreak. This mutant contains an amino acid substitution at position 82 (A82V) and has been reported to be associated with increased infectivity and pathogenicity (Diehl et al., 2016; Dietzel et al., 2017; Hoffmann et al., 2017). We transfected 293T and HeLa cells to express EBOV-GP that circulated in the beginning of the West Africa outbreak (Makona variant) or the A82V mutant (Figures 6C and 6D). Strikingly, the A82V variant secreted GP-virosomes in a highly efficient manner superior to the parental WT GP. In 293T cells, GP-virosome release was completely blocked by transfected tetherin (Figure 6C). In contrast in HeLa cells, expressing endogenous levels of tetherin, the A82V mutant facilitated GP-virosome release with high efficiency in comparison with WT GP (Figure 6D). Altogether, GP derived from highly pathogenic EBOV strains is more efficiently secreted as GP-virosomes in comparison with GP from low- or non-pathogenic strains.

GP-Virosomes Are Decoys for EBOV-Neutralizing Antibodies and Have Immunomodulatory Functions

Secretory vesicles bearing GP might trap EBOV-neutralizing antibodies. To test for this, we established a neutralization assay on

the basis of production of GP-pseudotyped MLV particles encoding for the firefly luciferase as reporter for transduction (Figure 7A). We mixed GP-pseudotyped MLV particles with growth medium or the conditioned supernatant of 293T cells previously transfected to express GFP alone, EBOV-GP+GFP or EBOV-GP+tetherin. These supernatants contain no GP-virosomes (GFP), high levels of GP-virosomes (GP+GFP), or reduced levels of GP-virosomes due to tetherin co-expression (GP+tetherin). Next, we added increasing amounts of KZ52, a neutralizing GP antibody, which is derived from a survivor of the 1995 Kikwit EVD outbreak (Maruyama et al., 1999), to these mixtures and incubated them for 1 h, before they were inoculated onto naive 293T cells. Finally, firefly luciferase activity in the lysates of transduced cells was measured at 72 h post-transduction. MLV EBOV-GP-mediated transduction of cells treated with DMEM or concentrated supernatants containing no GP-virosomes (GFP) was sensitive to neutralization by KZ52 in a concentration-dependent manner (Figure 7A). This phenotype was GP specific, because MLV VSV-G pseudotypes were largely resistant against neutralization. Strikingly, GP-virosomes (GP+GFP) counteracted the neutralizing activity of the KZ52 antibody at 0.1 and 1 $\mu\text{g/mL}$. This suggests that GP-virosomes have the capacity to trap EBOV-neutralizing antibodies. In contrast, tetherin expression (GP+tetherin) restored the neutralizing activity of the KZ52 antibody, presumably through suppression of GP-virosome release (Figure 7A).

MLV particles bearing GP might not faithfully reflect the biology of filamentous EBOV particles. Therefore, we performed the identical experiment except for replacing the MLV pseudotypes with the EBOV-like particles generated in the trVLP system, which allows the study of authentic EBOV morphogenesis, budding, and entry (Watt et al., 2014). As expected, increasing amounts of the KZ52 antibody potentially neutralized EBOV-trVLP infection (Figure 7B). Furthermore, and in agreement with the results obtained with EBOV-GP-pseudotyped MLV, cell culture supernatants containing GP-virosomes counteracted the neutralizing activity of KZ52 up to concentrations of 10 $\mu\text{g/mL}$ antibody (Figure 7B). Co-expression of tetherin in the virosome-producing cells restored antibody neutralization. Hence, GP-virosomes incorporate antigenically intact GP, which captures EBOV-neutralizing antibodies.

Virosomes bearing EBOV-GP could contribute to EBOV pathogenicity by exerting immunomodulatory activity. Furthermore, tetherin could antagonize such an effect by inhibition of virosome release. To analyze this, we treated primary human monocyte-derived macrophages with concentrated supernatants from

Nuclei of cells were visualized with DAPI. For each condition, the absolute number of PLA spots in ten transfected (GFP+) cells were counted. To test for statistical significance, a one-way ANOVA with Dunn's multiple-comparison test was used (* $p < 0.05$ and *** $p < 0.001$). Scale bar, 40 μm .

(D) Similar experimental setup as in (C), but GP-expressing plasmids without GFP were used and instead of the PLA probes secondary antibodies counterstained tetherin (Alexa 633) and GP (Alexa 488). Shown are representative of at least ten images per condition. Scale bar, 40 μm .

(E) 293T cells were transfected to express tetherin and the indicated V5-tagged GP-variants. 24 hours post-transfection, cells were lysed and the GPs were immunoprecipitated with a V5-specific antibody. V5-GP as well as tetherin in input lysates (left) as well as the precipitate (right) were analyzed using western blot.

(F) 293T cells were transfected to express EBOV-GP or the ELE variant together with tetherin or a non-coding control plasmid. 24 hours post-transfection, GP levels in cell culture media and cell lysates as well as tetherin levels in the cell lysates were analyzed using western blot.

(G) HeLa cells were transfected to express EBOV-GP or the ELE variant together with a tetherin-specific siRNA or a non-targeting siRNA as negative control. 24 hours post-transfection, GP levels in cell culture media and cell lysates were quantified using western blot. For each set of data, the results were verified in at least three independent experiments.

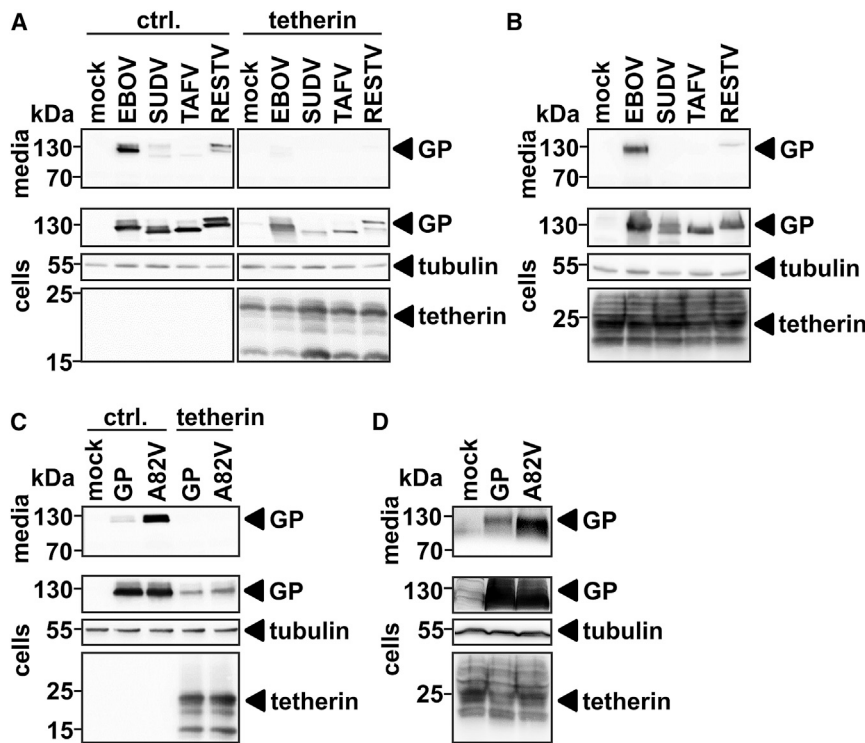


Figure 6. Ebola virus GP Release Is Associated with Increased Viral Pathogenicity

(A) 293T cells were transfected to express EBOV-GP, SUDV-GP, TAFV-GP, or RESTV-GP together with tetherin or a non-coding control plasmid. 24 hours post-transfection, GP levels in cell culture media and cell lysates as well as tetherin levels in the cell lysates were determined using western blot.

(B) HeLa cells were transfected to express EBOV-GP, SUDV-GP, TAFV-GP, or RESTV-GP, and GP levels in cell culture media and cell lysates were quantified using western blot.

(C) 293T cells were transfected to express EBOV-GP or the GP-A82V variant derived from the 2014 Ebola outbreak in West Africa together with tetherin or a non-coding control plasmid. 24 hours post-transfection, GP levels in cell culture media and cell lysates as well as tetherin levels in the cell lysates were determined using western blot.

(D) HeLa cells were transfected to express EBOV-GP or the GP-A82V variant and GP levels in cell culture media and cell lysates were quantified using western blot. All results were verified in at least three independent experiments.

cells expressing GFP (no virosomes), GP+GFP (GP-virosomes), and GP+tetherin (GP-virosome release suppressed by tetherin) and monitored release of cytokines (Figure 7C). The cytokine secretion profile from the three different macrophage donors was quite variable, but from the 36 cytokines included in the array we identified 8 cytokines that were detectable in all measurements with similar trends. Release of CXCL1, MIP-1 α/β , IL-1RA, IL-8, and MIF was largely unaffected by GP-bearing virosomes. Conversely, secretion of CCL2, CCL5, and TNF- α was reduced upon treatment with supernatants containing GP-virosomes (Figure 7C). Of note, when macrophages were treated with supernatants from 293T cells transfected to coexpress GP and tetherin, the cytokine release pattern was comparable with macrophages treated with supernatants from GFP-only expressing cells. This suggests that GP-virosomes are immunomodulatory and that tetherin antagonizes this effect through direct inhibition of virosome release.

Altogether, GP-virosomes act as decoys for neutralizing antibodies and modulate cytokine release from myeloid cells. Tetherin directly antagonizes this EBOV immune evasion strategy through inhibition of GP-virosome release.

DISCUSSION

EBOV-GP is the only viral surface protein and mediates entry into target cells. In addition, soluble forms of GP are generated in infected cells that may have immunomodulatory functions (Dolnik et al., 2004, 2015; Escudero-Pérez et al., 2014; Volchkov et al., 1998). Here, we present a comprehensive analysis of EBOV-GP-bearing virosomes (i.e., microvesicles that are secreted

from GP-expressing cells and incorporate GP). The existence of such GP-virosomes was first demonstrated by the pioneering work of Volchkov et al (1998), but their biological activities as well as the determinants of GP-virosome formation have remained elusive. In the present study we identified determinants in GP that are important for GP-virosome release and show that tetherin inhibits release of GP-virosomes. Furthermore, our results support a role of GP-virosomes in pathogenicity and immune evasion of ebolaviruses.

We identified single amino acid residues in the RBD that are important for GP-virosome formation (Figures 5A and 5B). Notably, the same residues have been previously demonstrated to be involved in GP-mediated entry and tetherin antagonism but were dispensable for GP virion incorporation and augmentation of VP40-driven VLP release (Brinkmann et al., 2016). A thus far unknown RBD-binding partner is supposed to be involved in GP-driven entry (Dube et al., 2008, 2010) and tetherin counteraction (Brinkmann et al., 2016), and according to our results the same factor might also be involved in regulating GP-virosome release. It remains enigmatic how RBD-dependent GP-virosome release might be linked to viral entry. However, it is tempting to speculate that secretion of virosomes could be related to GP-mediated tetherin antagonism. Because GP-virosomes are sensitive to inhibition by tetherin, they might trap tetherin molecules on the cell surface that would otherwise inhibit release of viral progeny. On the other hand, mutation of a GXXXA motif in the GP-TMD has little impact on viral infectivity, impairs GP-mediated tetherin antagonism (González-Hernández et al., 2018), but has no impact on GP-virosome formation (Figures 5A and 5B). This demonstrates that formation of GP-virosomes, tetherin

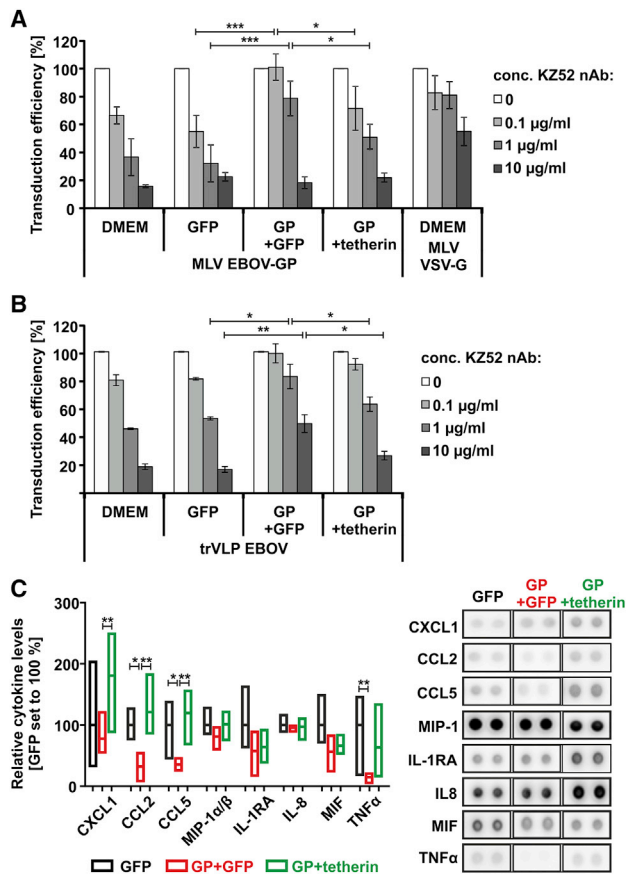


Figure 7. GP-Virosomes Are Decoys for EBOV-Neutralizing Antibodies and Have Immunomodulatory Functions

(A) 293T cells were transduced with MLV-pseudotypes bearing EBOV-GP or VSV-G, mixed with the indicated cell culture supernatants and the indicated amounts of EBOV-GP-neutralizing antibody (KZ52). The transduction efficiency of MLV pseudotypes mixed with the indicated supernatants in the absence of antibody was set to 100%. Shown is the mean relative transduction efficiency (SEM, $n = 5$, triplicate transductions). We used a two-way ANOVA with Dunnett's multiple-comparison test to determine statistical significance ($*p < 0.05$ and $***p < 0.001$).

(B) Similar setup as in (A), but 293T cells were transduced with transcription and replication competent EBOV-like particles (trVLP) and mixed with the indicated cell culture supernatants and increasing amounts of the KZ52 antibody. The transduction efficiency of trVLPs mixed with the indicated supernatants in the absence of antibody was set to 100%. Shown is the mean relative transduction efficiency (SEM, $n = 3$, triplicate transductions). We used a two-way ANOVA with Dunnett's multiple-comparison test to determine statistical significance ($*p < 0.05$ and $**p < 0.01$).

(C) Primary human monocyte-derived macrophages were treated with the indicated cell culture supernatants. 24 hours later, relative cytokine levels were quantified with a cytokine array. The floating bar plot shows the mean as well as minimum and maximum levels for each cytokine measured from experiments with three independent macrophage donors. We used a two-way ANOVA with Fisher's least significant difference (LSD) test to determine statistical significance ($*p < 0.05$ and $**p < 0.01$). Right: representative primary array spots of the eight cytokines analyzed.

antagonism, and viral entry are mediated by overlapping although not identical GP domains and can be functionally separated.

GP-virosome release is negatively regulated by tetherin (Figure 3). Mechanistically this process is reminiscent to inhibition of viral particle release by tetherin. Tetherin acts like a clamp and inserts its TMD into the membrane of budding viral particles and connects them to the cellular plasma membrane via the GPI anchor, thereby suppressing virus release (Sauter, 2014). Similarly, tetherin without GPI anchor was inactive in suppression of GP-virosomes and was incorporated into released viral particles (Figure 4A). In line with this, tetherin has recently been implicated in the regulation of exosome secretion from HeLa cells (Edgar et al., 2016).

We analyzed tetherin orthologs from different species as well as an artificial tetherin that shares its domain organization with tetherin but has no sequence homology to tetherin. Although all these tetherin variants have been shown to potentially suppress viral particle release (Heusinger et al., 2015; Perez-Caballero et al., 2009), they varied substantially in their capability to interfere with GP-virosome formation (Figures 4C and 4D). For instance, alligator tetherin was expressed to lower levels than hamster or human tetherin but potentially blocked GP-virosomes. Furthermore, the artificial tetherin variant was expressed to very high amounts but was comparable with human tetherin and clearly inferior in its anti-GP-virosome activity to fruit bat tetherin. What is the underlying cause of this sequence specific element in tetherin's anti-GP-virosome activity? We postulate that specificity is conferred by the direct binding of GP to tetherin via its TMD. This is supported by functional analysis of a GP-chimeric protein expressing the LASV GP TMD (ELE). This GP chimera does not antagonize tetherin (Gnirß et al., 2014) and shows reduced binding to endogenous tetherin (Figure 5C), which could also explain why it is less sensitive to tetherin-mediated inhibition of GP-virosome formation (Figures 5F and 5G).

Release of subviral particles or virosomes devoid of viral nucleic acid is known from other viruses; for instance, HBV subviral particles act as decoys for neutralizing antibodies (Hu and Liu, 2017). We now demonstrate a similar activity for GP-virosomes (Figures 7A and 7B). Furthermore, we show that GP-virosomes are immunomodulatory, as they change the cytokine secretion pattern of macrophages (Figure 7C). This activity of GP-virosomes might help EBOV to evade the host's immune system and might contribute to viral pathogenicity.

A potential role of virosome formation in EBOV pathogenicity is supported by the observation that the GP from highly pathogenic EBOV strain responsible for the EVD outbreak in Zaire in 1976 and, particularly, the GP of the Makona variant responsible for the EVD epidemic in West Africa in 2014–2016 are superior in mediating GP-virosome formation compared with GPs of other ebolaviruses, including SUDV- and TAFV-GP (Figure 6). Tetherin, as part of the antiviral innate immune response, might interfere with GP-virosome formation and help the immune system control systemic EBOV infection, independent of its effects on viral particle release. In line with such a scenario, tetherin derived from fruit bats, presumably the natural reservoir of EBOV, inhibited GP-virosome release with high efficiency (Figure 4D).

Altogether, EBOV-GP, in its microvesicle-associated form, might represent a previously non-perceived determinant of EBOV pathogenicity. Moreover, the antiviral factor tetherin suppresses release of viral microvesicles and could thereby antagonize the deleterious effects of viral infection, suggesting

that the role of tetherin in innate immune control could be even broader than anticipated.

STAR★METHODS

Detailed methods are provided in the online version of this paper and include the following:

- **KEY RESOURCES TABLE**
- **CONTACT FOR REAGENT AND RESOURCE SHARING**
- **EXPERIMENTAL MODEL AND SUBJECT DETAILS**
 - Cells and cell culture
- **METHOD DETAILS**
 - Plasmids, antibodies and siRNA
 - Transfection of 293T and HeLa cells
 - Transduction of HeLa and THP-1-shSamHD1 cells
 - Concentration of vesicles from the culture supernatant
 - Cell lysis and extraction of total protein
 - Western blot analysis
 - Co-Immunoprecipitation
 - Proximity ligation assay (PLA)
 - Confocal microscopy
 - 3D-SIM super resolution live cell imaging
 - Electron microscopy
 - GP-based neutralization assay
 - Detection of cytokine levels
- **QUANTIFICATION AND STATISTICAL ANALYSIS**

SUPPLEMENTAL INFORMATION

Supplemental Information includes four figures and four videos and can be found with this article online at <https://doi.org/10.1016/j.celrep.2019.01.065>.

ACKNOWLEDGMENTS

We would like to thank Gerhard Jahn and Thomas Ifner for constant support and encouragement and Ulrike Protzer for providing continued access to the research facilities at the Helmholtz Center Munich. Furthermore, we thank Daniel Sauter, Paul Bieniasz, and Thomas Gramberg for providing reagents and Thomas Hoenen for the trVLP system. This work was funded by grants to S.P. and M. Schindler from Deutsche Forschungsgemeinschaft (SCHI 1073/4-1 and PO 716/8-1). Furthermore, M. Schindler received institutional support from the Helmholtz Center Munich, German Research Center for Environmental Health, and the University Hospital Tuebingen.

AUTHOR CONTRIBUTIONS

J.N., R.B., M.H., C.B., B.F., S.H., S.P., and M. Schindler designed experiments. J.N., R.B., M.H., C.B., B.F., B.M., C.S., and D.K. performed the experiments. J.N., R.B., M.H., C.B., B.F., D.K., S.H., S.P., and M. Schindler analyzed the data. M.H., M. Schaller, S.P., and M. Schindler contributed reagents and analysis tools. J.N., R.B., and M. Schindler wrote the manuscript. M. Schindler conceived the overall study and developed the manuscript to its final form.

DECLARATION OF INTERESTS

The authors declare no competing interests.

Received: December 12, 2017
Revised: November 7, 2018
Accepted: January 16, 2019
Published: February 12, 2019

REFERENCES

- Bartosch, B., Dubuisson, J., and Cosset, F.L. (2003). Infectious hepatitis C virus pseudo-particles containing functional E1-E2 envelope protein complexes. *J. Exp. Med.* 197, 633–642.
- Baseler, L., Chertow, D.S., Johnson, K.M., Feldmann, H., and Morens, D.M. (2017). The pathogenesis of Ebola virus disease. *Annu. Rev. Pathol.* 12, 387–418.
- Bhattacharyya, S., Warfield, K.L., Ruthel, G., Bavari, S., Aman, M.J., and Hope, T.J. (2010). Ebola virus uses clathrin-mediated endocytosis as an entry pathway. *Virology* 401, 18–28.
- Brinkmann, C., Nehlmeier, I., Walendy-Gnirß, K., Nehls, J., González Hernández, M., Hoffmann, M., Qiu, X., Takada, A., Schindler, M., and Pöhlmann, S. (2016). The tetherin antagonism of the Ebola virus glycoprotein requires an intact receptor-binding domain and can be blocked by GP1-specific antibodies. *J. Virol.* 90, 11075–11086.
- Buceta, J., and Johnson, K. (2017). Modeling the Ebola zoonotic dynamics: interplay between enviroclimatic factors and bat ecology. *PLoS ONE* 12, e0179559.
- Chahar, H.S., Bao, X., and Casola, A. (2015). Exosomes and their role in the life cycle and pathogenesis of RNA viruses. *Viruses* 7, 3204–3225.
- Dahlmann, F., Biedenkopf, N., Babler, A., Jahn-Dechent, W., Karsten, C.B., Gnirß, K., Schneider, H., Wensch, F., O'Callaghan, C.A., Bertram, S., et al. (2015). Analysis of Ebola virus entry into macrophages. *J. Infect. Dis.* 212 (Suppl 2), S247–S257.
- de La Vega, M.A., Stein, D., and Kobinger, G.P. (2015). Ebolavirus evolution: past and present. *PLoS Pathog.* 11, e1005221.
- Diehl, W.E., Lin, A.E., Grubaugh, N.D., Carvalho, L.M., Kim, K., Kyawe, P.P., McCauley, S.M., Donnard, E., Kucukural, A., McDonel, P., et al. (2016). Ebola virus glycoprotein with increased infectivity dominated the 2013–2016 epidemic. *Cell* 167, 1088–1098.e6.
- Dietzel, E., Schudt, G., Kräling, V., Matrosovich, M., and Becker, S. (2017). Functional characterization of adaptive mutations during the West African Ebola virus outbreak. *J. Virol.* 91, e01913–16.
- Dolnik, O., Volchkova, V., Garten, W., Carbonnelle, C., Becker, S., Kahnt, J., Ströher, U., Klenk, H.D., and Volchkov, V. (2004). Ectodomain shedding of the glycoprotein GP of Ebola virus. *EMBO J.* 23, 2175–2184.
- Dolnik, O., Volchkova, V.A., Escudero-Perez, B., Lawrence, P., Klenk, H.D., and Volchkov, V.E. (2015). Shedding of Ebola virus surface glycoprotein is a mechanism of self-regulation of cellular cytotoxicity and has a direct effect on virus infectivity. *J. Infect. Dis.* 212 (Suppl 2), S322–S328.
- Dube, D., Schornberg, K.L., Stantchev, T.S., Bonaparte, M.I., Delos, S.E., Bouton, A.H., Broder, C.C., and White, J.M. (2008). Cell adhesion promotes Ebola virus envelope glycoprotein-mediated binding and infection. *J. Virol.* 82, 7238–7242.
- Dube, D., Schornberg, K.L., Shoemaker, C.J., Delos, S.E., Stantchev, T.S., Clouse, K.A., Broder, C.C., and White, J.M. (2010). Cell adhesion-dependent membrane trafficking of a binding partner for the ebolavirus glycoprotein is a determinant of viral entry. *Proc. Natl. Acad. Sci. U S A* 107, 16637–16642.
- Edgar, J.R., Manna, P.T., Nishimura, S., Banting, G., and Robinson, M.S. (2016). Tetherin is an exosomal tether. *eLife* 5, e17180.
- Escudero-Pérez, B., Volchkova, V.A., Dolnik, O., Lawrence, P., and Volchkov, V.E. (2014). Shed GP of Ebola virus triggers immune activation and increased vascular permeability. *PLoS Pathog.* 10, e1004509.
- Gnirß, K., Fiedler, M., Krämer-Kühl, A., Bolduan, S., Mittler, E., Becker, S., Schindler, M., and Pöhlmann, S. (2014). Analysis of determinants in filovirus glycoproteins required for tetherin antagonism. *Viruses* 6, 1654–1671.
- González-Hernández, M., Hoffmann, M., Brinkmann, C., Nehls, J., Winkler, M., Schindler, M., and Pöhlmann, S. (2018). A GXXXA motif in the transmembrane domain of the Ebola virus glycoprotein is required for tetherin antagonism. *J. Virol.* 92, e00403–18.
- Gramberg, T., Hofmann, H., Möller, P., Lator, P.F., Marzi, A., Geier, M., Krum-biegel, M., Winkler, T., Kirchhoff, F., Adams, D.H., et al. (2005). LSECtin

interacts with filovirus glycoproteins and the spike protein of SARS coronavirus. *Virology* 340, 224–236.

Gramberg, T., Kahle, T., Bloch, N., Wittmann, S., Müllers, E., Daddacha, W., Hofmann, H., Kim, B., Lindemann, D., and Landau, N.R. (2013). Restriction of diverse retroviruses by SAMHD1. *Retrovirology* 10, 26.

Hacke, M., Björkholm, P., Hellwig, A., Himmels, P., Ruiz de Almodóvar, C., Brügger, B., Wieland, F., and Ernst, A.M. (2015). Inhibition of Ebola virus glycoprotein-mediated cytotoxicity by targeting its transmembrane domain and cholesterol. *Nat. Commun.* 6, 7688.

Heusinger, E., Kluge, S.F., Kirchhoff, F., and Sauter, D. (2015). Early vertebrate evolution of the host restriction factor tetherin. *J. Virol.* 89, 12154–12165.

Hoffmann, M., Müller, M.A., Drexler, J.F., Glende, J., Erdt, M., Gützow, T., Losemann, C., Binger, T., Deng, H., Schwegmann-Weßels, C., et al. (2013). Differential sensitivity of bat cells to infection by enveloped RNA viruses: coronaviruses, paramyxoviruses, filoviruses, and influenza viruses. *PLoS ONE* 8, e72942.

Hoffmann, M., González Hernández, M., Berger, E., Marzi, A., and Pöhlmann, S. (2016). The Glycoproteins of all filovirus species use the same host factors for entry into bat and human cells but entry efficiency is species dependent. *PLoS ONE* 11, e0149651.

Hoffmann, M., Crone, L., Dietzel, E., Paijo, J., González-Hernández, M., Nehlmeier, I., Kalinke, U., Becker, S., and Pöhlmann, S. (2017). A polymorphism within the internal fusion loop of the Ebola virus glycoprotein modulates host cell entry. *J. Virol.* 91, e00177–17.

Hoffmann, M., Nehlmeier, I., Brinkmann, C., Krähling, V., Behner, L., Moldenhauer, A.S., Krüger, N., Nehls, J., Schindler, M., Hoenen, T., et al. (2019). Tetherin Inhibits Nipah Virus but Not Ebola Virus Replication in Fruit Bat Cells. *J. Virol.* 93, e01821–18. <https://www.ncbi.nlm.nih.gov/pubmed/30429347?dopt=Abstract>.

Hu, J., and Liu, K. (2017). Complete and incomplete hepatitis B virus particles: formation, function, and application. *Viruses* 9, E56.

Ito, H., Watanabe, S., Takada, A., and Kawaoka, Y. (2001). Ebola virus glycoprotein: proteolytic processing, acylation, cell tropism, and detection of neutralizing antibodies. *J. Virol.* 75, 1576–1580.

Kaletsky, R.L., Francica, J.R., Agrawal-Gamse, C., and Bates, P. (2009). Tetherin-mediated restriction of filovirus budding is antagonized by the Ebola glycoprotein. *Proc. Natl. Acad. Sci. U S A* 106, 2886–2891.

Kalra, S., Kelkar, D., Galwankar, S.C., Papadimos, T.J., Stawicki, S.P., Arquilla, B., Hoey, B.A., Sharpe, R.P., Sabol, D., and Jahre, J.A. (2014). The emergence of Ebola as a global health security threat: from ‘lessons learned’ to coordinated multilateral containment efforts. *J. Glob. Infect. Dis.* 6, 164–177.

Koppensteiner, H., Banning, C., Schneider, C., Hohenberg, H., and Schindler, M. (2012). Macrophage internal HIV-1 is protected from neutralizing antibodies. *J. Virol.* 86, 2826–2836.

Kühl, A., Banning, C., Marzi, A., Votteler, J., Steffen, I., Bertram, S., Glowacka, I., Konrad, A., Stürzl, M., Guo, J.T., et al. (2011). The Ebola virus glycoprotein and HIV-1 Vpu employ different strategies to counteract the antiviral factor tetherin. *J. Infect. Dis.* 204 (Suppl 3), S850–S860.

Kupzig, S., Korolchuk, V., Rollason, R., Sugden, A., Wilde, A., and Banting, G. (2003). Bst-2/HM1.24 is a raft-associated apical membrane protein with an unusual topology. *Traffic* 4, 694–709.

Lai, F.W., Lichty, B.D., and Bowdish, D.M. (2015). Microvesicles: ubiquitous contributors to infection and immunity. *J. Leukoc. Biol.* 97, 237–245.

Le Guenno, B., Formenty, P., Wyers, M., Gounon, P., Walker, F., and Boesch, C. (1995). Isolation and partial characterisation of a new strain of Ebola virus. *Lancet* 345, 1271–1274.

Lee, J.E., and Saphire, E.O. (2009). Ebolavirus glycoprotein structure and mechanism of entry. *Future Virol.* 4, 621–635.

Lötvall, J., Hill, A.F., Hochberg, F., Buzás, E.I., Di Vizio, D., Gardiner, C., Gho, Y.S., Kurochkin, I.V., Mathivanan, S., Quesenberry, P., et al. (2014). Minimal experimental requirements for definition of extracellular vesicles and their

functions: a position statement from the International Society for Extracellular Vesicles. *J. Extracell. Vesicles* 3, 26913.

Mahauad-Fernandez, W.D., and Okeoma, C.M. (2015). The role of BST-2/tetherin in host protection and disease manifestation. *Immun. Inflamm. Dis.* 4, 4–23.

Manicassamy, B., Wang, J., Jiang, H., and Rong, L. (2005). Comprehensive analysis of ebola virus GP1 in viral entry. *J. Virol.* 79, 4793–4805.

Martinez, O., Ndungo, E., Tantral, L., Miller, E.H., Leung, L.W., Chandran, K., and Basler, C.F. (2013). A mutation in the Ebola virus envelope glycoprotein restricts viral entry in a host species- and cell-type-specific manner. *J. Virol.* 87, 3324–3334.

Maruyama, T., Rodriguez, L.L., Jahrling, P.B., Sanchez, A., Khan, A.S., Nichol, S.T., Peters, C.J., Parren, P.W., and Burton, D.R. (1999). Ebola virus can be effectively neutralized by antibody produced in natural human infection. *J. Virol.* 73, 6024–6030.

Meckes, D.G., Jr., and Raab-Traub, N. (2011). Microvesicles and viral infection. *J. Virol.* 85, 12844–12854.

Mehedi, M., Falzarano, D., Seebach, J., Hu, X., Carpenter, M.S., Schnittler, H.J., and Feldmann, H. (2011). A new Ebola virus nonstructural glycoprotein expressed through RNA editing. *J. Virol.* 85, 5406–5414.

Mohan, G.S., Li, W., Ye, L., Compans, R.W., and Yang, C. (2012). Antigenic subversion: a novel mechanism of host immune evasion by Ebola virus. *PLoS Pathog.* 8, e1003065.

Mühlberger, E. (2007). Filovirus replication and transcription. *Future Virol.* 2, 205–215.

Neil, S.J., Zang, T., and Bieniasz, P.D. (2008). Tetherin inhibits retrovirus release and is antagonized by HIV-1 Vpu. *Nature* 451, 425–430.

Ning, Y.J., Deng, F., Hu, Z., and Wang, H. (2017). The roles of ebolavirus glycoproteins in viral pathogenesis. *Virol. Sin.* 32, 3–15.

Parren, P.W.H.I., Geisbert, T.W., Maruyama, T., Jahrling, P.B., and Burton, D.R. (2002). Pre- and Postexposure Prophylaxis of Ebola Virus Infection in an Animal Model by Passive Transfer of a Neutralizing Human Antibody. *J. Virol.* 76, 6408–6412.

Perez-Caballero, D., Zang, T., Ebrahimi, A., McNatt, M.W., Gregory, D.A., Johnson, M.C., and Bieniasz, P.D. (2009). Tetherin inhibits HIV-1 release by directly tethering virions to cells. *Cell* 139, 499–511.

Pourrut, X., Souris, M., Towner, J.S., Rollin, P.E., Nichol, S.T., Gonzalez, J.P., and Leroy, E. (2009). Large serological survey showing cocirculation of Ebola and Marburg viruses in Gabonese bat populations, and a high seroprevalence of both viruses in *Rousettus aegyptiacus*. *BMC Infect. Dis.* 9, 159.

Sanchez, A., Trappier, S.G., Mahy, B.W., Peters, C.J., and Nichol, S.T. (1996). The virion glycoproteins of Ebola viruses are encoded in two reading frames and are expressed through transcriptional editing. *Proc. Natl. Acad. Sci. USA* 93, 3602–3607.

Sauter, D. (2014). Counteraction of the multifunctional restriction factor tetherin. *Front. Microbiol.* 5, 163.

Schindler, M., Würfl, S., Benaroch, P., Greenough, T.C., Daniels, R., Easterbrook, P., Brenner, M., Münch, J., and Kirchhoff, F. (2003). Down-modulation of mature major histocompatibility complex class II and up-regulation of invariant chain cell surface expression are well-conserved functions of human and simian immunodeficiency virus nef alleles. *J. Virol.* 77, 10548–10556.

Ströher, U., West, E., Bugany, H., Klenk, H.D., Schnittler, H.J., and Feldmann, H. (2001). Infection and activation of monocytes by Marburg and Ebola viruses. *J. Virol.* 75, 11025–11033.

Szatanek, R., Baran, J., Siedlar, M., and Baj-Krzyworzeka, M. (2015). Isolation of extracellular vesicles: determining the correct approach (review). *Int. J. Mol. Med.* 36, 11–17.

Thery, C., Amigorena, S., Raposo, G., and Clayton, A. (2006). Isolation and characterization of exosomes from cell culture supernatants and biological fluids. *Curr. Protoc. Cell Biol. Chapter 3*, Unit 3.22.

Towner, J.S., Sealy, T.K., Khristova, M.L., Albariño, C.G., Conlan, S., Reeder, S.A., Quan, P.L., Lipkin, W.I., Downing, R., Tappero, J.W., et al. (2008). Newly

- discovered ebola virus associated with hemorrhagic fever outbreak in Uganda. *PLoS Pathog.* 4, e1000212.
- Van Damme, N., Goff, D., Katsura, C., Jorgenson, R.L., Mitchell, R., Johnson, M.C., Stephens, E.B., and Guatelli, J. (2008). The interferon-induced protein BST-2 restricts HIV-1 release and is downregulated from the cell surface by the viral Vpu protein. *Cell Host Microbe* 3, 245–252.
- Vande Burgt, N.H., Kaletsky, R.L., and Bates, P. (2015). Requirements within the Ebola viral glycoprotein for tetherin antagonism. *Viruses* 7, 5587–5602.
- Volchkov, V.E., Volchkova, V.A., Slenczka, W., Klenk, H.D., and Feldmann, H. (1998). Release of viral glycoproteins during Ebola virus infection. *Virology* 245, 110–119.
- Volchkov, V.E., Volchkova, V.A., Muhlberger, E., Kolesnikova, L.V., Weik, M., Dolnik, O., and Klenk, H.D. (2001). Recovery of infectious Ebola virus from complementary DNA: RNA editing of the GP gene and viral cytotoxicity. *Science* 291, 1965–1969.
- Volchkova, V.A., Feldmann, H., Klenk, H.D., and Volchkov, V.E. (1998). The nonstructural small glycoprotein sGP of Ebola virus is secreted as an antiparallel-orientated homodimer. *Virology* 250, 408–414.
- Wahl-Jensen, V., Kurz, S., Feldmann, F., Buehler, L.K., Kindrachuk, J., DeFilippis, V., da Silva Correia, J., Früh, K., Kuhn, J.H., Burton, D.R., and Feldmann, H. (2011). Ebola virion attachment and entry into human macrophages profoundly effects early cellular gene expression. *PLoS Negl. Trop. Dis.* 5, e1359.
- Watt, A., Moukambi, F., Banadyga, L., Groseth, A., Callison, J., Herwig, A., Ebihara, H., Feldmann, H., and Hoenen, T. (2014). A novel life cycle modeling system for Ebola virus shows a genome length-dependent role of VP24 in virus infectivity. *J. Virol.* 88, 10511–10524.
- Witwer, K.W., Buzás, E.I., Bemis, L.T., Bora, A., Lässer, C., Lötvall, J., Nolte-'t Hoen, E.N., Piper, M.G., Sivaraman, S., Skog, J., et al. (2013). Standardization of sample collection, isolation and analysis methods in extracellular vesicle research. *J. Extracell. Vesicles* 2, 2.
- Wensch, F., Karsten, C.B., Gnirß, K., Hoffmann, M., Lu, K., Takada, A., Winkler, M., Simmons, G., and Pöhlmann, S. (2015). Interferon-induced transmembrane protein-mediated inhibition of host cell entry of Ebolaviruses. *J. Infect. Dis.* 212 (Suppl 2), S210–S218.

STAR★METHODS

KEY RESOURCES TABLE

REAGENT or RESOURCE	SOURCE	IDENTIFIER
Antibodies		
Rabbit-anti-GP1	Wrensch et al., 2015	PMID: 26034199
Rabbit-anti-GP2	Icosagen	Cat#A2-100-100
KZ52 EBOV neutralizing antibody	Parren et al., 2002 ; provided by S. Becker	PMID: 12021376
Mouse-anti-Tetherin	Abnova	Cat#H00000684-B02P; RRID:AB_1204015
Rabbit-anti-Tetherin	NIH AIDS Reagent Program	Cat#11721
Mouse-anti-Flag (F-tag-01)	Abcam	Cat#ab18230; RRID:AB_444336
Rabbit-anti-V5	Abcam	Cat#ab9116; RRID:AB_307024
Rabbit-anti-alpha-tubulin	Thermo	Cat#PA5-22060; RRID:AB_11154084
Rabbit-anti-HA	Thermo	Cat#71-5500; RRID:AB_2533988
Mouse-anti-Actin	Sigma	Cat#A3853; RRID:AB_262137
Mouse-anti-CD81 (clone B11)	SantaCruz	Cat#sc-166029; RRID:AB_2275892
Mouse-anti-TSG101 (clone C2)	SantaCruz	Cat#sc-7964; RRID:AB_671392
Mouse-anti-Calnexin (clone AF18)	SantaCruz	Cat#sc-23954; RRID:AB_626783
HRP-conjugated goat anti-mouse	Dianova	Cat#A21010 RRID:AB_2728771
HRP-conjugated goat anti-rabbit	Dianova	Cat#A21020
Goat-anti-Rabbit 800CW	Li-Cor	Cat#926-32211; RRID:AB_621843
Goat-anti-Mouse 680RD	Li-Cor	Cat#926-68070; RRID:AB_10956588
Rabbit polyclonal V5 (CoLP)	Diagenode	#C15410270
Bacterial and Virus Strains		
NEB stable competent E.coli	NEB	Cat#C3040H
Chemicals, Peptides, and Recombinant Proteins		
Puromycin	Thermo	Cat#A11138-03
Lipofectamin2000	Thermo	Cat#11668019
Saponin	Applichem	Cat#A4518,0100
Protease inhibitor cocktail (Complete Mini)	Roche	Cat#04693124001
Critical Commercial Assays		
Proteome Profiler Human Cytokine Array Kit Panel A	R&D Systems	Cat#ARY005B
Duolink <i>In Situ</i> Detection Reagents Red	Sigma-Aldrich	Cat#DUO92008
Duolink <i>In Situ</i> PLA Probe Anti-Rabbit PLUS	Sigma-Aldrich	Cat#DUO92002
Duolink <i>In Situ</i> PLA Probe Anti-Mouse MINUS	Sigma-Aldrich	Cat#DUO92004
Cell Culture Lysis Reagent	Promega	Cat#E1531
Beetle-Juice BIG KIT	PJK	Cat#102511
Renilla luciferase: coelenterazine	Roth	Cat#4094.4
Experimental Models: Cell Lines		
293T cells (embryonal kidney)	DSMZ	Cat#ACC635
HeLa cells (cervix carcinoma)	DSMZ	Cat#ACC57
THP-1-shSamHD1	Gramberg et al., 2013	PMID: 23497255
Oligonucleotides		
Fwd_EBOV_GP_XbaI: 5'-CGTCTAGAATATGGGCGTTAGAGGAAT ATTGC-3'	This paper	N/A
Rev_EBOV_GP_MluI: 5'-TACGCGTTTCTAAAAGACAAATTTCAT ATACAG-3'	This paper	N/A

(Continued on next page)

Continued

REAGENT or RESOURCE	SOURCE	IDENTIFIER
Fwd_tetherinΔGPI_Xbal: 5'-CGTCTAGAATATGGCATCTACTTCG TATG-3'	This paper	N/A
Rev_tetherinΔGPI_MluI: 5'-CTACGCGTTTAGCTGGAGTCCTGG GAG-3'	This paper	N/A
Fwd_EBOV_GP2014_Xbal: 5'-CGTCTAGAATATGGGTGTTACA GGAATATTGC-3'	This paper	N/A
Rev_EBOV_GP2014_MluI: 5'-TACGCGTTTCTAAAAGACAAATTT GCATATACAG-3'	This paper	N/A
Fwd_pWPXLd_GP_GFP_BamHI: GCAGGATCCATGGGCGTTAC AGGAATATTGC	This paper	N/A
Rev_pWPXLd_GP_GFP_MluI: GTCACGCGTCCAAAGACAAATT TGCATATA	This paper	N/A
Fwd_pWPXLd_GP_BamHI: GCAGGATCCATGGGCGTTACAGG AATATTGC	This paper	N/A
Rev_pWPXLd_GP_EcoRI: GCAAGGAATTCCTAAAAGACAAATT TGCATATAC	This paper	N/A
Recombinant DNA		
pCG-IRES-GFP	Schindler et al., 2003	PMID: 12970439
artificial tetherin and human tetherin (pCAGGS backbone)	Perez-Caballero et al., 2009	PMID: 19879838
Human, hamster, alligator X2 tetherin (pCG-IRES-GFP backbone)	Heusinger et al., 2015	PMID: 26401043
Hyp and Epo tetherin	Hoffmann et al., 2019	PMID: 30429347; MG792836, MG792837
V5-tagged EBOV-GP, LASV-GPC, ELE-GP and LEL-GP chimeras (pCAGGS backbone)	Gnirß et al., 2014	PMID: 24721789
GP LXXXL (pCAGGS backbone)	Hacke et al., 2015	PMID: 26158910
GP WT (Mayinga) and RBD mutants (F88A, L111A, L122A, W104A) (all in pCDNA3 backbone)	Brinkmann et al., 2016	PMID: 27707924
RESTV-, SUDV-, TAFV-GP (pCAGGS backbone)	Hoffmann et al., 2016	PMID: 26901159
GP 2014 and GP A82V (pCAGGS backbone)	Hoffmann et al., 2017	PMID: 28228590
Above mentioned GP-variants in the pCG-IRES-GFP backbone	This paper	
pWPXLd		Addgene Plasmid #12258
psPAX2		Addgene Plasmid #12260
pMD2.G		Addgene Plasmid #12259
MLV-gag/pol, MLV-luc provided by G. Simmons (Blood Systems Research Institute, San Francisco, California)	Bartosch et al., 2003	PMID: 12615904
pCAGGS-based expression plasmids for EBOV-NP, EBOV-VP30, EBOV-VP35, EBOV-L, trVLP minigenome and T7-polymerase	Watt et al., 2014	PMID: 24965473
Human DC-SIGN (pCDNA3 backbone)	Gramberg et al., 2005	PMID: 16051304
Software and Algorithms		
ImageStudio	Li-Cor	Li-Cor
Velocity 2.0 Software	PerkinElmer	PerkinElmer
DeltaVision Image Acquisition Software	GE Healthcare	GE Healthcare
ImageJ	ImageJ	https://imagej.net/Downloads
ImageJ Plugin "Bleach Correction"	ImageJ	https://imagej.net/Bleach_Correction
PlateReaderSoftware Version 0.5.41.0	Hidex	Hidex
Other		
SMARTpool On-TARGET BST2 siRNA	Dharmacon	L-011817-00-0005
SMARTpool non-targeting siRNA	Dharmacon	D-001810-10-20
Sepharose beads (Sephacrose 6B)	Sigma-Aldrich	Cat#6B100
Protein G Sepharose	Thermo Fisher Scientific	Cat#20397

CONTACT FOR REAGENT AND RESOURCE SHARING

Further information and requests for resources and reagents should be directed to and will be fulfilled by the Lead Contact, Michael Schindler (michael.schindler@med.uni-tuebingen.de).

EXPERIMENTAL MODEL AND SUBJECT DETAILS

Cells and cell culture

HEK293T and HeLa cells were grown in DMEM (Thermo Fisher or Biochrom) supplemented with 10% heat-inactivated fetal calf serum (FCS), 2 mM L-Glutamine and 100 µg/ml Penicillin/Streptomycin in a humidified cell culture incubator at 37°C and 5% CO₂. THP-I-shSamHD1 ([Gramberg et al., 2013](#)), which were used to enhance the lentiviral transduction efficiency, were cultured in RPMI containing 0.25 µg/ml Puromycin and supplemented with 10% FCS, 2 mM L-Glutamine and 100 µg/ml Penicillin/Streptomycin.

METHOD DETAILS

Plasmids, antibodies and siRNA

The EBOV-GP expression plasmid was generated by amplification of the GP cDNA sequence of the EBOV Mayinga strain by PCR (forward 5'-CGTCTAGAATATGGGCGTTAGAGGAATATTGC-3' and reverse 5'-TACGCGTTTCTAAAAGACAAATTTGCATATACAG-3') and subsequent insertion into the pCG-IRES-GFP plasmid using the restriction enzymes MluI and XbaI. GFP is expressed independently from this plasmid via an internal ribosomal entry site (IRES) and allows for the fluorescence-based detection of transfected cells. The tetherin expression plasmid was generated by amplifying the human tetherin cDNA sequence (forward 5'-CGTCTAGAATATGGCATCTACTTCGTATG and reverse 5'-CTACGCGTCACTGCAGCAGAGCGCTGAGGC-3') inserting it into the pCG plasmid with or without IRES-GFP via MluI and XbaI restriction sites. The tetherinΔGPI, tetherinΔTMD and tetherinΔGPIΔTMD mutants were generated by mutagenesis PCR (forward 5'-CGTCTAGAATATGGCATCTACTTCGTATG-3' and reverse 5'-CTACGCGTTAGCTGGAGTCCTGGGAG-3') and subsequent cloning into the pCG vector via MluI and XbaI. The human, hamster (GREG), alligator X2 and artificial tetherin expression plasmids were kindly provided by D. Sauter and P. Bieniasz ([Heusinger et al., 2015](#); [Perez-Caballero et al., 2009](#)). Fruit bat tetherins, Epo and Hyp tetherin, where cloned from fruit bat cell lines EpoNi/22.1 and HypNi/1.1 ([Hoffmann et al., 2013](#)), respectively, and sequences have been submitted to GenBank under accession numbers MG792836 and MG792837. The plasmids coding for the GP RBD mutants (F88A, L111A, L122A, W104A), GP LXXL, LASV-GPC, ELE and LEL GP chimera, wild-type GP as well as the GP A82V mutant derived from the 2014 Ebola outbreak in West Africa are described elsewhere ([Brinkmann et al., 2016](#); [Gnirß et al., 2014](#); [Hacke et al., 2015](#); [Hoffmann et al., 2017](#)). The GP-coding sequences of those mutants were amplified by PCR (forward 5'-CGTCTAGAATATGGGTGTTACAGGAATATTGC-3' and reverse 5'-TACGCGTTTCTAAAAGACAAATTTGCATATACAG-3') and subsequently cloned into the pCG-IRES-GFP vector using the restriction enzymes MluI and XbaI. Plasmids encoding for RESTV-, SUDV-, TAFV-GP are described elsewhere ([Hoffmann et al., 2016](#)). To generate GP-GFP-expressing lentiviruses, we amplified GP with primers (forward 5'-GCAGGATCCATGGGCGTTACAGGAATATTGC-3' and reverse 5'-GTCACGCGTCCAAAGACAAATTTGCATATA-3') introducing a 5'-BamHI site and a 3'-MluI removing the stop codon and further allowing in frame insertion of GP to the GFP ORF within the pWPXLd (received from Addgene plasmid #12258) lentiviral backbone. pWPXLd only expressing GP was generated by amplification of GP with primers (forward 5'-GCAGGATCCATGGGCGTTACAGGAATATTGC-3' and reverse 5'-GCAAGGAATTCCTAAAAGACAAATTTGCATATAC-3') introducing a 5'-BamHI site and a 3'-EcoRI site and replacement of GFP with the GP ORF. All PCR amplified fragments were sequenced to confirm nucleotide identity.

For the detection of GP, a previously described polyclonal serum was used, which was raised in rabbits and targets the GP1-subunit ([Wrensch et al., 2015](#)). The rabbit anti-tetherin antibody was obtained from the NIH AIDS reagent program. The following antibodies were obtained commercially: polyclonal rabbit anti-GP2 (Icosagen, A2-100-100), polyclonal mouse anti-tetherin (Abnova, H00000684-B02P), monoclonal mouse anti-Flag (Abcam, ab18230), rabbit anti-V5 (Abcam, ab9116), polyclonal rabbit anti-α-tubulin (Invitrogen, PA5-22060), polyclonal rabbit anti-HA (Invitrogen, 71-5500), monoclonal mouse anti-Actin (Sigma, A3853), monoclonal mouse anti-CD81 (SantaCruz, B11, sc-166029), monoclonal mouse anti-TSG101 (SantaCruz, C2, sc-7964), monoclonal mouse anti-Calnexin (SantaCruz, AF18, sc-23954) and the secondary HRP-conjugated anti-mouse and anti-rabbit antibodies (Dianova) as well as the goat anti-rabbit 800CW (Li-Cor) and goat-anti-mouse RD680 (Li-Cor).

The SMARTpool On-TARGET plus tetherin-targeting siRNA, which provides a mixture of four different oligonucleotides (BST2: L-011817-00-0005), as well as the SMARTpool non-targeting control siRNA (Control: D-001810-10-20) was purchased from Dharmacon.

Transfection of 293T and HeLa cells

293T cells were transfected with plasmid DNA via calcium phosphate. One day before transfection, 1.5×10^5 293T cells were plated into 12-well plates. The next day, the transfection reaction was prepared by adding 3 µg of plasmid DNA and 6.5 µl 2 M CaCl₂ to ddH₂O ad 50 µl. The solution was subsequently combined with 50 µl 2 x HBS and vigorously mixed for 10 s. After incubation for

20 min at room temperature (RT), the transfection reaction was added to the cells dropwise. The culture medium was replaced 6 hpt and the cells were cultured for at least another 18 h before cells analysis.

HeLa cells were transfected with plasmid DNA or siRNA using Lipofectamine 2000 according to the manufacturer's instructions. Briefly, 2×10^5 cells were plated into 12-well plates. The next day, the transfection reaction was set up according to the manufacturer's protocol using 3 μ l of Lipofectamine 2000 and 1.6 μ g plasmid DNA or 40 pmol siRNA. After 15 min, the transfection reaction was added to the cells for 6 h. 18 h later cells were harvested and analyzed.

Transduction of HeLa and THP-I-shSamHD1 cells

To produce lentiviral stocks, 0.45×10^6 293T cells were seeded on a 6-well plate. 3 μ g pWPXLd, 2.25 μ g psPAX2 and 0.9 μ g pMD2G were transfected using 8 μ l Lipofectamine 2000 according to the manufacturer's protocol. 5 h later medium was changed and stocks were harvested after additional 24 h. 0.25×10^6 HeLa or 1×10^6 THP-I-shSamHD1 cells (treated with 30 ng/ml PMA) were seeded on a 6-well plate and transduced the next day. Lentiviral stock was spinoculated for 2 h 1 200 rpm at 25°C. Afterward the cell cultures were shifted to 37°C and medium was changed 24 hpi. Cells and supernatants were harvested for western blot analysis 3 dpi.

Concentration of vesicles from the culture supernatant

For analysis of secreted microvesicles, the supernatant was collected 24 hpt and pre-cleared at 8 000 x g for 10 minutes to pellet dead cells and cell debris. Subsequently, the supernatant was centrifuged for 2 h at 21 000 x g and 4°C. Afterward, the supernatant was removed and the pellet resuspended in 25 μ l 1 x Laemmli buffer containing 10% β -mercaptoethanol. The proteins were finally denatured at 95°C for 5 minutes. If larger volumes of culture supernatant were processed, the supernatant was first concentrated twenty-times by centrifugation at 5 000 x g for 30 min using Pierce Protein Concentrators with a MWCO of 30 kDa (Thermo Fisher). Afterward, the microvesicles within the retentate were pelleted as described above.

Cell lysis and extraction of total protein

Western blot samples were harvested 24 hpt. The cells were washed twice with PBS and subsequently pelleted by centrifugation at 7 000 x g for 5 minutes. Afterward, the supernatant was aspirated and the pellet was lysed in 30 μ l standard RIPA-buffer (150 mM NaCl, 50 mM Tris (pH = 8), 1% NP40, 0.5% sodium deoxycholate, 0.1% SDS). Following incubation for 30 min at 4°C, cell debris and insoluble proteins were spun down at 20 000 x g for 10 min and the supernatant was mixed with 5 x Laemmli buffer containing 10% β -mercaptoethanol. Finally, the proteins were boiled at 95°C for 5 min.

Western blot analysis

Cellular proteins as well as proteins released into the culture supernatant were separated according to their size by sodium dodecyl sulfate polyacrylamide gel electrophoresis (SDS-PAGE) using 12% or 15% polyacrylamide gels. Following SDS-PAGE, the proteins were blotted onto nitrocellulose membranes using a wet transfer or semidry system. The membranes were subsequently blocked for 1 h at RT in blocking solution (powdered milk in PBST). After blocking, the membranes were incubated with the diluted primary antibodies for 16 h at 4°C under gentle agitation. The rabbit anti-GP1, rabbit anti-tetherin, rabbit anti-HA and mouse anti-Flag antibodies were diluted 1:2 000 in blocking solution, the rabbit anti- α -tubulin and mouse anti-actin antibody 1:1 000 and the rabbit anti-GP2 antibody 1:500. Further antibodies were diluted as following: mouse anti-CD81 (1:100), mouse anti-TSG101 (1:200), mouse anti-Calnexin (1:200).

Afterward, the membranes were washed three times with 0.1% Tween-20 in PBS (PBST). Protein detection was either achieved by chemiluminescence or fluorescence. For chemiluminescence, the membranes were incubated in HRP-conjugated secondary anti-mouse or anti-rabbit antibodies (diluted 1:5 000 in blocking solution) for 1 h at RT. Next, the membranes were washed three times with PBST. For staining of the blots, ECL developing solution was prepared by adding 10 μ l 30% H_2O_2 and 100 μ l of 0.2 mM p-coumaric acid in DMSO to 10 mL of 1.25 mM Luminol in 1 M Tris (pH 8.5). The membranes were incubated for 5 min in ECL developing solution and chemiluminescent signals were detected and analyzed using the Fusion FX7 camera system.

In case of fluorescence staining, the membranes were incubated in goat anti-rabbit 800CW (diluted 1:15 000 in PBST) or goat anti-mouse 680RD (diluted in 1:15 000 in PBST) for 1 h at RT. After a final washing step with PBST, the membranes were analyzed using FcOdysee (Li-Cor) and ImageStudio (Li-Cor).

Co-Immunoprecipitation

For co-immunoprecipitation, 1×10^6 transiently transfected HEK293T cells were lysed in 200 μ l of immunoprecipitation buffer (50 mM Tris (pH 7.4), 1% Triton X-100, 150 mM NaCl, 5 mM Na_3VO_4 , 5 mM Na_2PO_7 , 5 mM NaF and protease inhibitor cocktail). Lysates were precleared for 1 h at 4°C with empty Sepharose beads. Immunoprecipitation was performed at 4°C for 1 h using 2 μ g of the anti-V5 antibody. Thereafter, lysates were incubated with protein G Sepharose for 1 h at 4°C, extensively washed in lysis buffer, resolved on an SDS-PAGE and immunostained for the relevant protein.

Proximity ligation assay (PLA)

Potential protein-protein interactions between tetherin and wild-type GP or ELE GP were analyzed using the Duolink Proximity Ligation Assay (PLA) Red Mouse/Rabbit kit (Sigma-Aldrich). 1×10^5 HeLa cells were plated into 12-well plates on coverslips and

transfected with the indicated expression plasmids as described above. 24 hpt, the coverslips were washed twice with PBS and the cells were fixed in 2% PFA in PBS for 30 min at 4°C. Afterward, the cells were treated with 1% Saponin in PBS for 10 min at room temperature to permeabilize the plasma membrane. Following permeabilization, the cells were blocked with 10% heat-inactivated FCS in PBS for 1 h at RT and subsequently incubated with the primary antibody solution for 1 h at RT in a humidified chamber. The rabbit anti-GP1 antibody was diluted 1: 500 and the mouse anti-tetherin antibody 1: 100 in 1% heat-inactivated FCS in PBS. Binding of the PLA-probes, ligation of the oligonucleotides, rolling-circle amplification and mounting of the coverslips was performed as described in the manufacturer's protocol.

Confocal microscopy

Following staining, the cells were imaged with a 60 x objective lens using a confocal spinning-disc Nikon Ti Eclipse microscope equipped with an UltraView VoX system (Perkin Elmer). The images were processed and PLA spot counts were determined using the Volocity 2.0 software.

3D-SIM super resolution live cell imaging

HeLa cells were seeded and THP-1-shSamHD1 cells were PMA-differentiated on Wilco-dishes. Transduction of the cells was essentially done as described before but without spinoculation of the cells. 3 or 4 days post transduction cells were imaged under live conditions (37°C, 5% CO₂, phenolred free medium) with the DeltaVision OMX SR imaging system (GE Healthcare). Images were taken for 2 min every 20 s. Subsequent image analysis was done using SoftWorx and ImageJ. All image sequences were corrected for bleaching running the ImageJ plugin "Bleach Correction."

Electron microscopy

To reduce background, exosome-depleted medium was used in electron microscopy analysis. Supplemented medium containing 20% FCS was ultracentrifuged (100 000 x g) over night at 4°C. The supernatant was diluted to a final FCS concentration of 10% and used to culture transfected HeLa cells. 0.1x 10⁶ HeLa cells were seeded on 12-well plates and transfected with pCAGGS-ZEBOV-GP-V5 or the respective control plasmid by using Lipofectamine 2000 as described above. Medium was changed 5 hpt. 2 dpt, cells were harvested by accutase treatment. PBS washed cell pellets were fixed with Karnovsky's solution for 24 h at 4°C. Afterward, cell pellets were embedded in 3.5% agarose at 37°C, coagulated at RT, and fixed again in Karnovsky's solution. Post-fixation was based on 1.0% osmium tetroxide containing 1.5% K-ferrocyanide in 0.1 M cacodylate buffer for 2 h. Following standard methods, blocks were embedded in glycidic ether and cut using an ultra microtome (Ultracut, Reichert). Ultra-thin sections (30 nm) were mounted on copper grids and analyzed using a Zeiss LIBRA 120 transmission electron microscope (Zeiss) operating at 120 kV.

At the same time point supernatants were harvested, cleared from cells (300 x g for 10 min) and cellular debris (2 600 x g for 7 min). Afterward the supernatant containing vesicles and virus-like particles was fixed by adding the same volume of 4% PFA in 0.1 M HEPES for 15 min at RT. Further on, the supernatant was centrifuged at 21 000 x g for 2 h at 4°C. Resulting pellets were resuspended in 80 µl fixation solution (2% PFA in 0.05 M HEPES) which was directly placed onto a glow-discharged EM grid. After adsorption, grids were washed in PBS, stained for 15 min with rabbit anti-V5 antibody (1:50), washed in PBS followed by 6 nm gold-conjugated goat anti-rabbit IgG (Jackson ImmunoResearch Laboratories), washed in PBS and negatively stained with 1% uranyl acetate. The grids were examined using a Zeiss LIBRA 120 transmission electron microscope (Zeiss) operating at 120 kV.

GP-based neutralization assay

For the production of MLV-based pseudotype particles (MLVpp), 293T cells were transfected with plasmids encoding MLV-gag/pol, MLV-luc and the indicated GP or empty vector as control, using the calcium phosphate method. At 16 hpt, the transfection medium was changed to normal growth medium (DMEM [PAN] + 10% FBS [Biochrom], 100 µg/ml Penicillin/Streptomycin [PAN]). MLVpp-containing supernatants were harvested at 60 hpt, cleared of cellular debris via centrifugation (4,000 x g, 10 min) and filtered through a sterile filter (0.45 µm pore size, Merck Millipore). Transcription- and replication-competent EBOV-like particles (trVLPs) were produced according to a published protocol (Watt et al., 2014). Briefly, 293T cells were transfected with pCAGGS-based expression plasmids EBOV-NP, EBOV-VP30, EBOV-VP35, EBOV-L, T7-polymerase and T7-promotor-controlled trVLP minigenome, using the calcium phosphate method. At 16 hpt, the transfection medium was changed to normal growth medium. Culture supernatants containing trVLP were harvested at 60 hpt and cleared from cellular debris by centrifugation (4,000 x g, 10 min). To test whether virocytes can reduce the sensitivity of GP-driven host cell entry to neutralization by EBOV-GP-specific antibodies, purified MLVpp or trVLP were mixed 1:1 with the supernatant of cells expressing EBOV-GP alone, EBOV-GP and human tetherin or GFP (no EBOV-GP control), or normal growth medium (no transfection control). Afterward, the mixtures were incubated for 1 h with increasing amounts (0.1, 1 and 10 µg/ml) of an antibody recognizing the neutralizing KZ52 epitope of EBOV-GP (kindly provided by Stephan Becker, Marburg), while samples incubated without antibody served as controls (maximum transduction control). Next, 50 µl of each sample were inoculated as triplicates on target cells grown in 96-well format. For transduction with MLVpp naive 293T cells served as target cells, whereas for transduction with trVLP, 293T cells that were previously (16 h in advance) transfected with expression plasmids for EBOV-NP, EBOV-VP30, EBOV-VP35, EBOV-L and human DC-SIGN were used. At 72 h post transduction, cell lysates were prepared by aspiration of the culture medium and incubation of the cells with Cell Culture Lysis Reagent (Promega, art. #E1531, final concentration 1x) for 30 min at room temperature. Next, lysates were transferred into white, opaque-walled 96-well plates before firefly

(MLVpp) or Renilla (trVLP) luciferase activity was quantified using a plate luminometer (Hidex Sense with PlateReaderSoftware version 0.5.41.0, Hidex) and commercial substrates (firefly luciferase: PJK, art. #102511; Renilla luciferase: coelenterazine [Carl Roth, art. #4094.4,] final concentration 20 μ M).

Detection of cytokine levels

Primary human macrophages were obtained from PBMC that were isolated from buffy coat by density gradient centrifugation essentially as described ([Koppensteiner et al., 2012](#)). Macrophages were allowed to differentiate three days in macrophage-specific medium (RPMI containing 4% human AB serum, 2 mM L-Glutamine, 100 μ g/ml Penicillin/Streptomycin, 1 mM Sodiumpyruvate, 1x non-essential amino acids and 0.4x MEM vitamins) and plastic adherence. After three days, non-adherent cells were removed and macrophages differentiate for additional four days in macrophage-specific medium.

1×10^5 macrophages were seeded per well of a 12 well plate. The next day, medium was replaced by a 1:2.5 diluted cell culture supernatant of either GFP, GP+GFP or GP+tetherin transfected 293T cells. 24 h later, the supernatants of macrophages were collected, centrifuged to remove cells and cell debris (3 200 x g 10 min) and subjected to the Proteome Profiler Human Cytokine Array Kit Panel A (ARY005B, R&D Systems) according to the manufacturer's protocol. All cytokine arrays were stained in parallel to avoid different exposure times. Cytokine spots were normalized to the reference control and calculated using the Dot blot Analyzer tool of ImageJ.

QUANTIFICATION AND STATISTICAL ANALYSIS

Statistical data analysis was done with GraphPad Prism (V6.0). For each figure the respective statistical parameters and tests used are indicated in the figure legend.

Cell Reports, Volume 26

Supplemental Information

Release of Immunomodulatory Ebola Virus

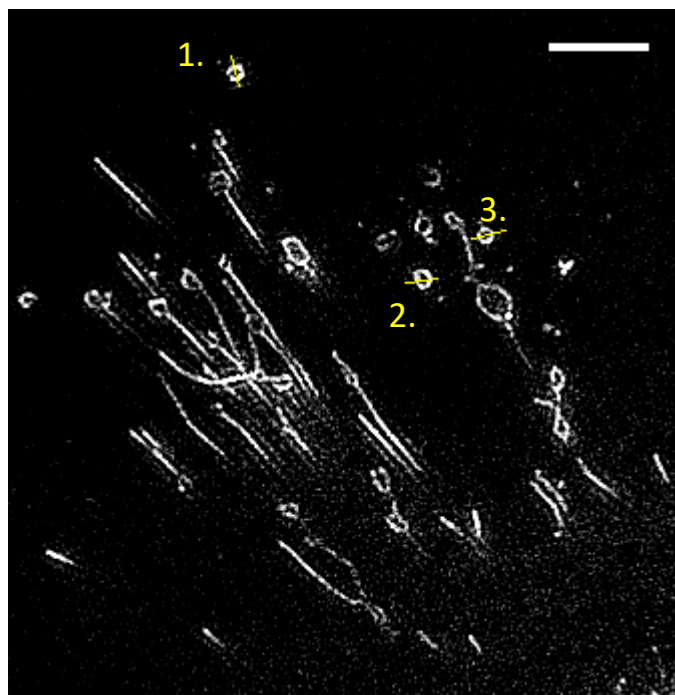
Glycoprotein-Containing Microvesicles Is Suppressed

by Tetherin in a Species-Specific Manner

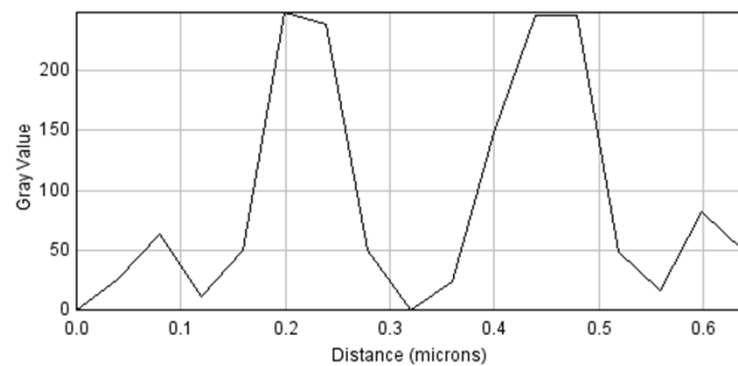
Julia Nehls, Ramona Businger, Markus Hoffmann, Constantin Brinkmann, Birgit Fehrenbacher, Martin Schaller, Brigitte Maurer, Caroline Schönfeld, Daniela Kramer, Stephan Hailfinger, Stefan Pöhlmann, and Michael Schindler

SUPPLEMENTAL FIGURES

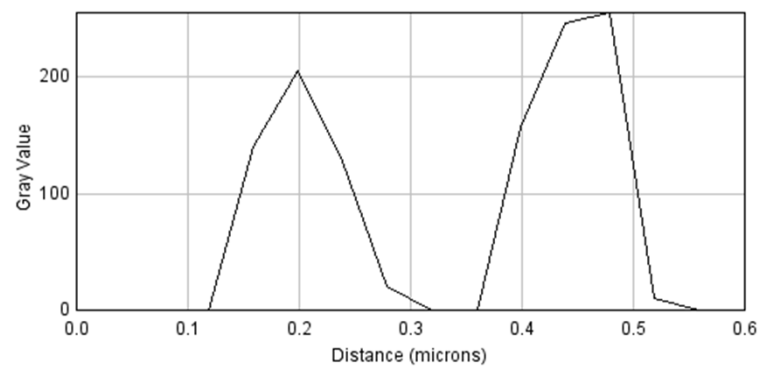
THP-I



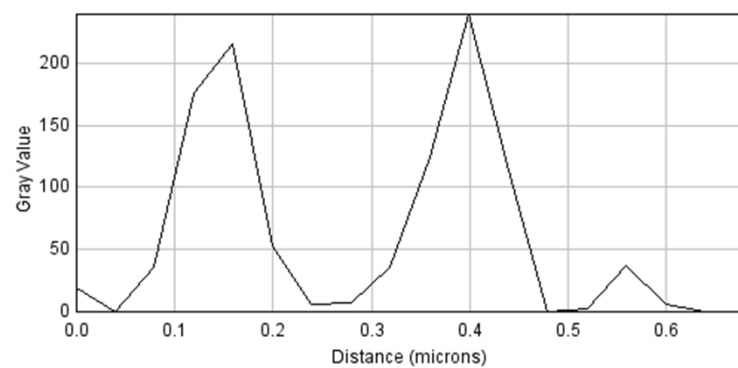
1.



2.

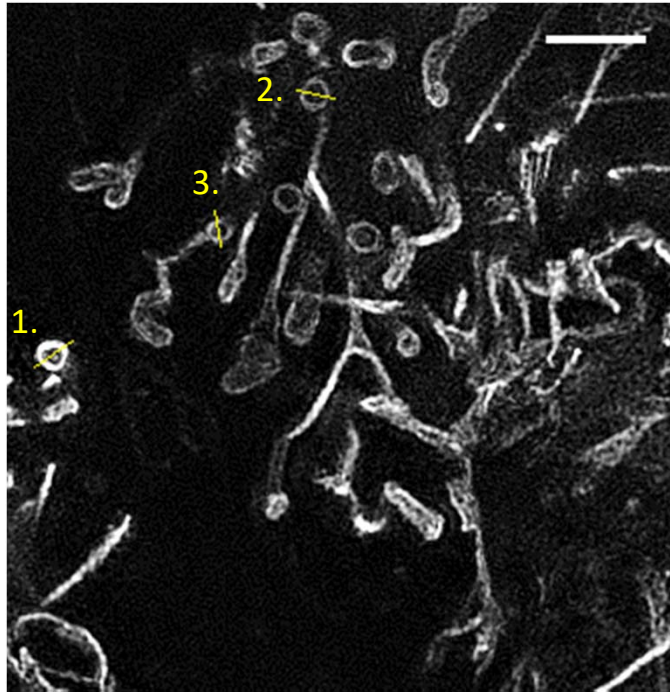


3.



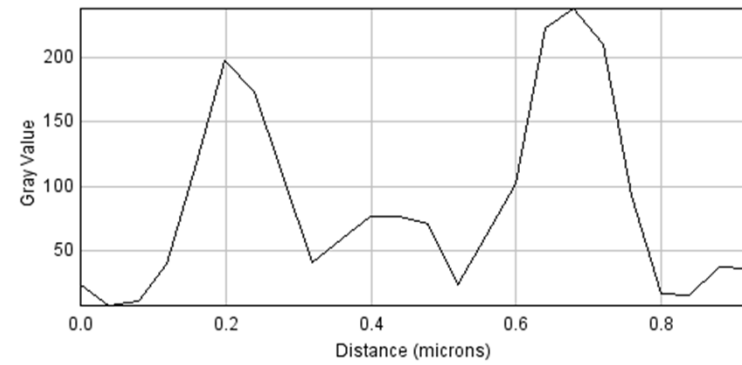
Supplemental Fig. 1 related to Fig. 2B and D: THP-I cells were transduced with GP-GFP expressing lentiviruses and analyzed by 3D-SIM live cell microscopy. Line profiles in the still images (compare Fig. 2B) were used to determine and quantify the size of GP-virosomes (compare Fig. 2D).

HeLa

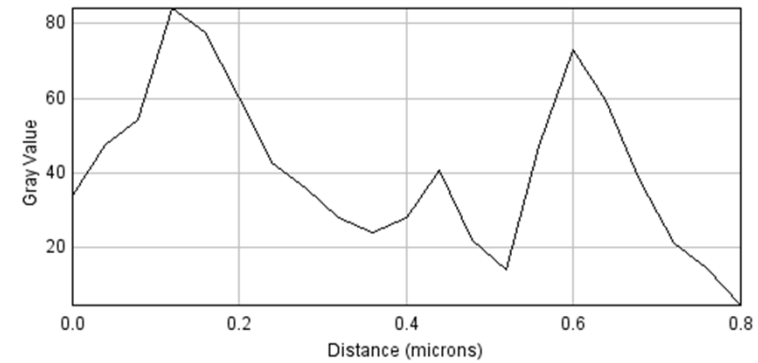


Supplemental Fig. 2 related to Fig. 2B and E: HeLa cells were transduced with GP-GFP expressing lentiviruses and analyzed by 3D-SIM live cell microscopy. Line profiles in the still images (compare Fig. 2B) were used to determine and quantify the size of GP-virosomes (compare Fig. 2E).

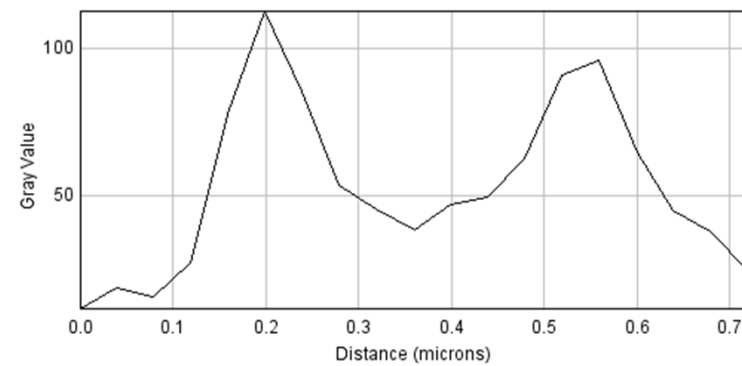
1.

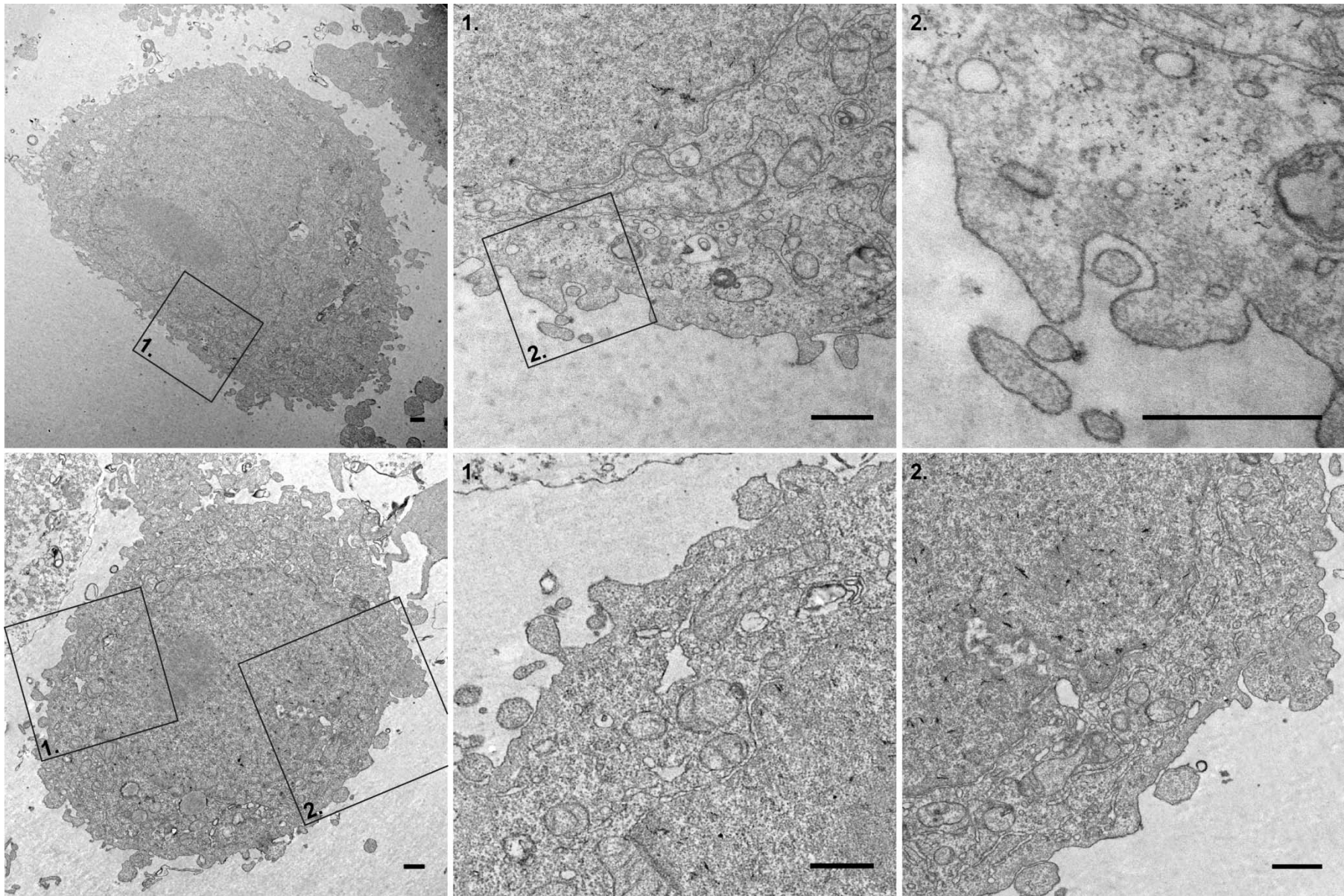


2.

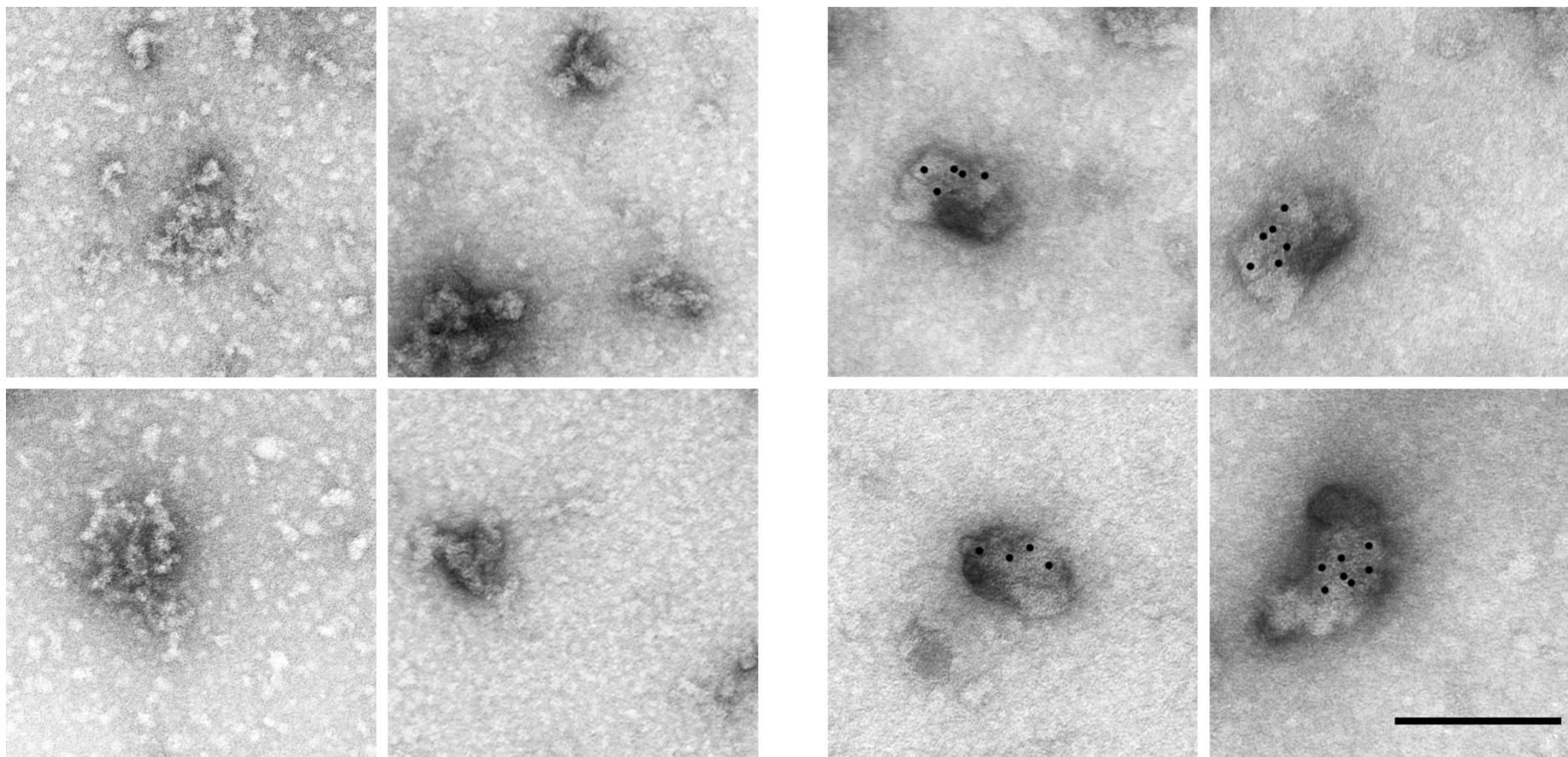


3.





Supplemental Fig. 3 related to Fig. 2F: Non GP-expressing control HeLa cells were analyzed by transmission electron microscopy (compare Fig. 2F). Specific areas visualizing microvesicles were cropped for magnification. Scale bar 500 nm.



Supplemental Fig. 4 related to Fig. 2Q and 2R: Ebola-GP immuno-gold staining of microvesicles produced from mock-transfected (left) or GP-expressing (right) HeLa cells (compare Fig. 2 Q/R). Scale bar 100 nm.